Decadal Variability in an Idealized Ocean Model and Its Sensitivity to Surface Boundary Conditions

A. CAPOTONDI* AND W. R. HOLLAND

National Center for Atmospheric Research+, Boulder, Colorado

(Manuscript received 5 January 1996, in final form 7 November 1996)

ABSTRACT

Variability in a three-dimensional ocean model of idealized geometry is analyzed. The variability is induced in the model by adding a stochastic component to the surface buoyancy forcing. The influence of the surface thermal forcing on the model variability is investigated under conditions in which the surface freshwater flux is specified. The thermal boundary conditions that have been considered include restoring boundary conditions with different restoring times, fixed surface heat flux, and boundary conditions derived by assuming an energy balance model for the atmosphere. It is found that the ocean model response varies considerably with the thermal boundary conditions used, given the specific ratio of thermal to haline forcing chosen for these calculations. A behavior characterized by sudden transitions between states of strong overturning and states of much weaker overturning dominates the model's response when a strong restoring is used, while quasi-regular oscillations at a period of approximately 24 years are found with boundary conditions that allow the sea surface temperature to respond to changes in the oceanic heat transport. The spatial pattern of the stochastic forcing is considered here as a variable of the problem, and the model's response to different spatial patterns is analyzed. The same decadal signal is found for all spatial patterns, suggesting that the variability at this timescale can be considered as an internal mode of the system and not associated with some characteristics of the forcing. However, different special patterns can be more or less effective in exciting the oceanic mode. Large-scale forcing directly contributing to the east–west pressure gradient appears to produce the largest response.

1. Introduction

Variability of the climate system at decadal timescales has emerged in recent studies of long term datasets (Deser and Blackmon 1993; Dickson et al. 1993; Levitus et al. 1994; Kushnir 1994). Most of these studies focus on the North Atlantic region, a region that plays a very important role in the global climate system and for which relatively dense datasets are available. In fact, deep-water formation in the northern North Atlantic drives an overturning circulation associated with transport of heat and salt from low to high latitudes, thus affecting the global heat budget. Also, the surface temperature and salinity distribution at high latitudes are linked to the rate of deep-water formation so that feedbacks between these surface properties and the strength of the overturning can be expected.

The analysis of sea surface temperature (SST) and sea level pressure (SLP) performed by Deser and Blackmon (1993), for example, shows the emergence of a mode of variability characterized by a dipole pattern with anomalies of one sign east of Newfoundland and anomalies of opposite polarity off the southeast coast of the United States. The timescales of the associated variability are quasi-biennal and quasi-decadal. From temperature records at Ocean Weather Station C (52°45′N, 35°30′W) it also appears that a quasi-decadal signal can be found down to a depth of about 125 m (Levitus et al. 1994).

It has also been speculated that events such as the ''Great Salinity Anomaly,'' a large upper-ocean freshwater mass that was observed to travel around the subpolar gyre during the period 1968–82 (Dickson et al. 1993), may be related to decadal-scale fluctuations of sea ice extent in the Greenland–Iceland Sea (Mysak et al. 1990).

Variability at interdecadal timescales has also been found in a coupled ocean–atmosphere model (Delworth et al. 1993). This variability, which has a period of approximately 50 years, is associated with changes in the strength of the meridional overturning. Although the coupled system includes a simple ice model of thermodynamic type (Bryan 1969), this component does not seem to play an active role in the dynamics of the 50-yr

*Current affiliation: Program in Atmospheric and Oceanic Sciences, University of Colorado at Boulder, Boulder, Colorado.

+The National Center for Atmospheric Research is sponsored by the National Science Foundation.

Corresponding author address: A. Capotondi, University of Colorado, Program in Atmospheric and Oceanic Sciences, Campus Box 311, Boulder, CO 80309.
E-mail: anton@ncar.ucar.edu

oscillation. Therefore, the question remains about the relative role of the oceanic and atmospheric components in determining the nature of the interdecadal variability: Is interdecadal variability an oceanic phenomenon, an atmospheric phenomenon, or a truly coupled mode of the system?

Griffies and Tziperman (1995) suggest that the variability observed in the coupled model by Delworth et al. (1993) can be interpreted as a linear mode of the ocean model excited by atmospheric forcing. In this scenario, the atmospheric component supplies the energy for the oscillation, but the timescale and the dynamics of the oscillation itself are dictated by the ocean. The argument is based upon an analogy between the ocean model of the coupled system and a hemispheric ocean box model for which a linear stability analysis is performed. In the parameter regime that allows the box model to mimic some of the results of the coupled model, linear modes of variability of the box model include damped oscillatory solutions. The application of a stochastic component to the surface thermal forcing results in an oscillatory behavior of the system (at the frequency of the damped oscillatory mode) with characteristics similar to the ones observed in the coupled model. Although very suggestive, the analogy is not yet conclusive, due to the simplicity of the box model compared to the three-dimensional oceanic component of the coupled system.

A different interpretation for the existence of spectral peaks in the variability of coupled systems can be made (Saravanan and McWilliams 1996b) by considering an advecting ocean dynamics and a localized atmospheric forcing with a given spatial scale. The oceanic advective velocity over the area of the forcing can give rise to a preferred timescale of variability (and corresponding spectral peak) without the existence of any intrinsic oscillatory mode in either system. In this scenario the preferred timescale of variability will depend on the spatial scale of the atmospheric forcing for a given oceanic advective velocity. The oceanic advective velocity should be the one associated with the thermohaline component of the circulation, and it can be estimated as an average velocity over the depth of the northward flowing branch of the conveyor belt. In the North Atlantic an estimate of the average velocity of the separated Gulf Stream over the top 400 m (Saravanan and McWilliams 1996b) is of the order of 1–2 cm s^{-1}. The variability in sea level pressure at decadal timescale, as emerged from the analysis of Deser and Blackmon (1993), shows a dipole structure covering the range of latitudes between 30° and 70°N so that the meridional length scale of atmospheric disturbances at the decadal scale can be estimated to be of the order of 4000 km. Thus, the timescale of oceanic advection through the area of atmospheric forcing is of the order of 8–16 years.

Variability at decadal and interdecadal scales has also been observed in three-dimensional ocean-only models (Weaver and Sarachik 1991; Weaver and Hughes 1994; Weaver et al. 1993, 1994; Greatbatch and Zhang 1995; Chen and Ghil 1995). These studies were carried out in coarse-resolution models with idealized sector geometry. Some of them (Weaver and Sarachik 1991; Weaver et al. 1993) use surface thermohaline boundary conditions known as ''mixed boundary conditions'' (the surface ocean temperature is restored toward a prescribed temperature field, while the surface boundary condition for salinity is in the form of a prescribed freshwater flux). A steady state is often never reached, and the system evolution may undergo oscillatory phases in the intensity of the thermohaline circulation at a quasi-decadal period. Greatbatch and Zhang (1995) find a sustained oscillation with a period of 32 years in a hemispheric planetary geostrophic model using a fixed heat flux as surface thermal boundary conditions (and no salinity effects included in the model). Chen and Ghil (1995) show that interdecadal self-sustained oscillations are obtained when the surface buoyancy forcing is characterized by either net evaporation or net cooling in northern high latitudes. The underlying dynamics of these oscillations is still unclear, and their dependence upon the parameter choices has not yet been fully investigated.

In this study we reconsider the question of the possible modes of variability of the ocean alone and carry out an exploration of some areas of parameter space. The model we use is a three-dimensional ocean model configured in an idealized sector geometry. The latter has been chosen because 1) the results can be more easily related to previous studies such as the ones mentioned above, and 2) the computational cost is sufficiently small to allow a more extensive sensitivity analysis. Based on the results of this study, some experiments are being repeated in a more realistic model of the North Atlantic. The results of the latter experiments and their comparison with observations will be presented in a subsequent paper.

The approach we have adopted for determining the modes of variability of the ocean model consists in perturbing the system (initially in a stable steady state) with a stochastic component added to the surface forcing. Since the variability of the forcing is white in frequency domain, the emergence of preferred scales of variability can only be attributed to the ocean dynamics, thus identifying modes of variability of the ocean model. The spatial distribution of the stochastic forcing is considered as a variable of the problem and the sensitivity of the results to different distributions is investigated. In particular, the system's response to differing spatial scales of forcing will help in understanding if the emergence of preferred timescales can be attributed to oscillatory modes of the ocean model or if it is the result of the coupling between oceanic advection and spatial structure of surface forcing as in Saravanan and the McWilliams (1996b) hypothesis.

Recent studies have shown that the equilibria of the thermohaline circulation as well as their stability char-

acteristics are strongly dependent upon the choice of the surface thermal boundary conditions (Zhang et al. 1993; Rahmstorf and Willebrand 1995). Therefore, the characteristics of the ocean model variability can also be expected to be dependent upon the thermal boundary conditions used. In this study we systematically investigate this dependence by considering several thermal boundary conditions differing in the degree to which they constrain the SST. To facilitate the comparison among the different boundary conditions the same mean state is considered in all cases. We will show that variability at decadal timescale can account for a large fraction of the variance in those cases in which the model SST has some freedom to respond to changes in the ocean circulation. The characteristics of the variability in these cases are described and compared by using an objective (empirical orthogonal function) analysis approach. The sensitivity of decadal variability to the surface thermal forcing as well as to the spatial distribution of the stochastic component of the forcing is the main emphasis of this paper. The dynamics associated with the decadal signal will be investigated in a subsequent paper.

The model (including surface thermal boundary conditions and characteristics of the stochastic forcing) is described in section 2, the model response to the stochastic forcing when different thermal boundary conditions and different stochastic forcing patterns are used is presented in section 3, and the results are discussed in section 4.

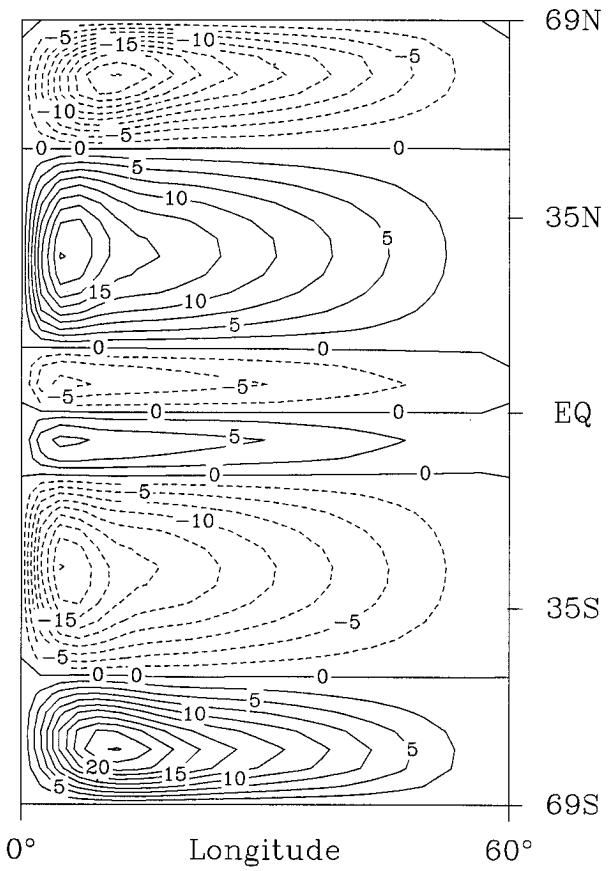

FIG. 1. Barotropic streamfunction (in Sv) for the initial state. The contour interval is 2.5 Sv.

2. The model

The model is the GFDL primitive equation model, based upon the work of Bryan (1969) and Cox (1984). The version used for this study follows the description given in Cox (1984), and the reader is referred to the latter for more information.

Our interest here is the identification of possible modes of variability of ocean models at decadal scales in the presence of a stochastic component in the surface forcing. As a first step we choose the simplest three-dimensional geometry for an ocean basin, a sector geometry, as shown in Fig. 1. The model domain extends from 69°S to 69°N and it is 60° wide in longitude. The horizontal resolution is 3° in the meridional direction, while in the zonal direction the resolution varies from 2° near the western boundary to 3° at the eastern boundary. There are 15 vertical levels, with resolution varying from 30 m at the top to 1000 m near the bottom. The model ocean has a constant depth of 5000 m.

The values of the mixing coefficients are in the range appropriate for coarse-resolution models (Bryan 1987). We have chosen values of $10^5 \text{m}^2\ \text{s}^{-1}$ and $4 \times 10^{-4} \text{m}^2\ \text{s}^{-1}$ for the horizontal and vertical viscosities, respectively, and $2 \times 10^3 \text{m}^2\ \text{s}^{-1}$ and $10^{-4} \text{m}^2\ \text{s}^{-1}$ for the horizontal and vertical diffusivities.

The parameterization of small-scale convective processes is accomplished according to the standard convective adjustment algorithm of the GFDL code (Cox 1984) using four passes (NCON = 4). For most of the calculations described in this paper we have used a linear equation of state in the form

$$\rho = \rho_o(T_o, S_o) + \alpha(T - T_o) + \beta(S - S_o), \quad (1)$$

where T and S are temperature and salinity, respectively, and T_o and S_o are their reference mean values, considered here as independent of depth. Here ρ_o is the corresponding reference density. Equation (1) is the linear truncation of the third-order polynomial approximation to the nonlinear equation of state according to Bryan and Cox (1972) (but ignoring compressibility effects). The values of the coefficients are $\alpha = -2 \times 10^{-4}$ g cm^{-3} °C^{-1} and $\beta = 8 \times 10^{-4}$ g cm^{-3} ppt^{-1}. We have chosen to use a linear equation of state for being able to more easily separate the effects of temperature from the effects of salinity. However, nonlinearities may be important at high latitudes where temperatures are low. In fact, the nonlinear character of the complete equation of state affects the relative importance of temperature and salinity variations in the buoyancy field, with temperature variations dominating the buoyancy field at high temperatures and salinity variations becoming rel-

atively more important at low temperatures. Therefore, we may overestimate the effect of temperature on the density field at high latitudes by using a linear equation of state. In order to assess the robustness of our results with respect to the form of the equation of state, a sensitivity experiment has been performed with a quadratic approximation in the form:

$$\rho = \rho_o(T_o, S_o) + \alpha(T - T_o) + \beta(S - S_o) + \gamma(T - T_o)^2, \quad (2)$$

where $\gamma = -4.5 \times 10^{-6}$ g cm^{-3} °C^{-2}. Equation (2) accounts for a large fraction of the nonlinearities at low temperatures. The results of the experiment using 2 are described in section 3e.

The surface forcing includes input of momentum by the wind. The wind stress is purely zonal, prescribed as a simple function of latitude (symmetrical with respect to the equator), and chosen to reproduce the major features of the observed wind distribution. The barotropic streamfunction obtained with this idealized wind is shown in Fig. 1.

Different surface thermal boundary conditions are considered as discussed in detail below. The surface boundary condition for salinity is specified in the form of a spatially varying, steady freshwater flux (or equivalent salt flux), expressing the negligible influence of sea surface salinity (SSS) on evaporation and precipitation. This choice does neglect the potentially important SST feedback on evaporation and hence precipitation. The spatial distribution of the surface freshwater flux has been diagnosed from an initial spinup phase, in which both temperature and salinity were relaxed toward prescribed temperature and salinity distributions (with a restoring timescale of 60 days for both quantities). The latter were both zonally uniform with a latitudinal dependence prescribed in the form of a cosine function with maximum at the equator. The temperature distribution varied from 28°C at the equator to 2°C at the northern and southern boundaries, while the salinity profile ranged from 37 ppt at the equator to 33 ppt at the northern and southern boundaries. At the end of the spinup a symmetric equilibrium state with sinking at both high latitudes was achieved. The corresponding (symmetric) equivalent salt flux was diagnosed and the simulation was continued with mixed boundary conditions (same restoring condition for temperature and flux boundary condition for salinity). The distribution of the equivalent salt flux is shown in Fig. 2. After switching to mixed boundary conditions, the SSS is no longer constrained to remain close to the given salinity distribution, but can respond to changes in the ocean circulation. Due to the positive feedback between SSS and thermohaline circulation (Bryan 1986; Willebrand 1993), small salinity perturbations at high latitudes can have a destabilizing effect on the symmetric thermal equilibrium. A ''polar halocline catastrophe'' (development of a halocline at high latitudes) (Bryan 1986) indeed occurred in our simulation, leading the model to evolve toward a new equilibrium characterized by sinking at high northern latitudes (pole-to-pole equilibrium). Some of the fields characterizing this equilibrium state are displayed in Fig. 3. The density distribution (top left) in the meridional–vertical plane is very homogeneous north of approximately 50°N where vigorous convection occurs. The velocity fields at 50-m and 4000-m depth (bottom panels) illustrate some aspects of the three-dimensional structure of the meridional overturning; close to the surface the northward flowing branch of the model conveyor belt appears as an enhanced northward flow in the western boundary current and northward flowing cross-equatorial flow. At depth, the southward return flow takes place in a deep western boundary current, as in the Stommel–Arons theory. The state in Fig. 3 has been used as the initial condition for the stochastically forced experiments that are described in section 3.

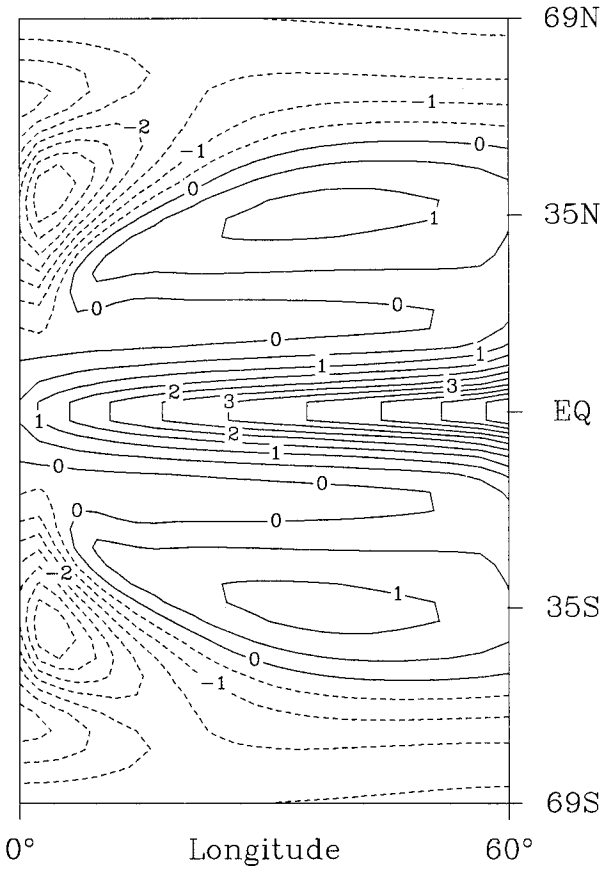

FIG. 2. Surface freshwater flux ($E - P$) in meters per year, diagnosed from the spinup. Contour interval is 0.5 m yr^{-1}

a. Surface stochastic forcing

Our purpose here is to perturb the system in such a way as to induce variability around the equilibrium state in Fig. 3. Since we want to identify the possible emergence of preferred oceanic timescales, we choose a per-

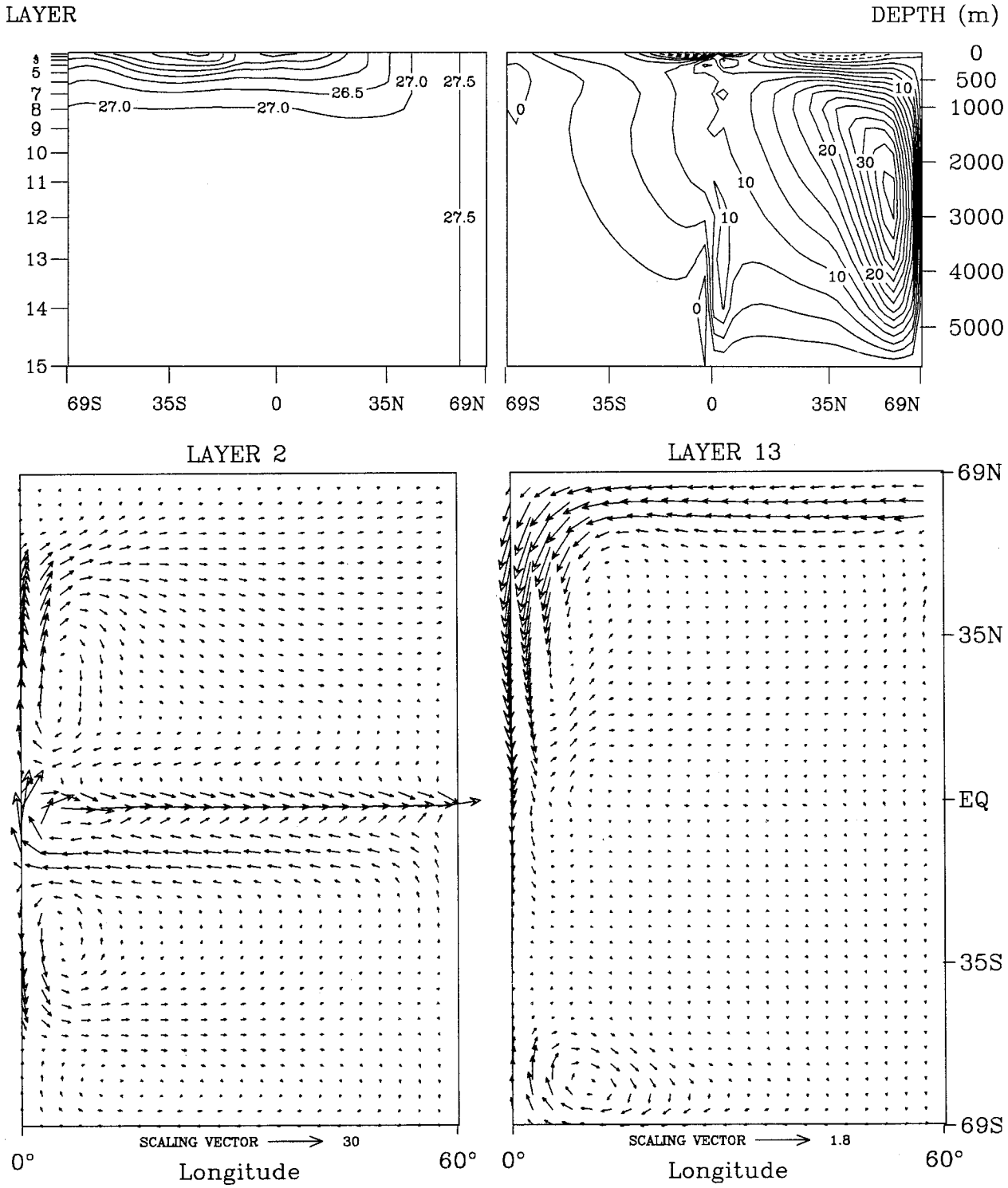

FIG. 3. Meridional section of density at 20° longitude (in sigma units, top left), meridional streamfunction (in Sv, top right), and horizontal velocity fields (in cm s^{-1}) at level 2 (bottom left) and level 13 (bottom right) for the pole-to-pole equilibrium state used as initial condition for the stochastically forced experiments.

turbation that is white in frequency domain. One option is to add a stochastic component to the surface thermal forcing (this has been the choice adopted by Griffies and Tziperman 1995), while the alternative option is to add the stochastic perturbation to the surface freshwater flux (an approach similar to the one used by Mikolajewicz and Maier-Reimer 1990). We first analyze the consequences of adding a stochastic component to the surface freshwater flux. Then, we consider how the system's response is altered when the perturbation is included in the thermal forcing.

The stochastic forcing is obtained by integrating a first-order Markovian process. A similar approach was used by Treguier and Hua (1987) and by Weaver et al. (1993). Here we follow the notation of Weaver et al. (1993). The equation governing the evolution of the random field F is

$$\frac{\partial F}{\partial t} = -\frac{F}{\tau_F} + \frac{S}{\hat{\tau}_F}, \tag{3}$$

where τ_F is the autocorrelation timescale of the process, $\hat{\tau}_F$ the timescale of the noise, and the noise field S is given by

$$S = \sum_{\kappa} \hat{S}(K) e^{i(\kappa \cdot x + \phi)}, \tag{4}$$

where $\hat{S}(K)$ is an isotropic spectrum, K is the wavenumber amplitude [$K = (\kappa \cdot \kappa)^{1/2}$], and ϕ is a random phase from 0 and 2π. The timescale of the noise has been chosen as

$$\hat{\tau}_F = (0.5 \Delta t \tau_F), \tag{5}$$

where Δt is the time step. A trapezoidal scheme has been used to advance (3). The one-sided frequency spectrum of the Markovian process is

$$|\tilde{F}|^2 = \frac{W}{(T_F f)^2 + 1}, \tag{6}$$

with f being the frequency, $T_F = 2\pi\tau_F$, and with W given by

$$W = 2\langle S^2 \rangle \tau_F^2 / \hat{\tau}_F^2. \tag{7}$$

Here $\langle S^2 \rangle$ is the variance of the white noise process. Thus, $|F|^2$ is a white spectrum for periods longer than T_F, while it decays as f^{-2} for periods shorter than T_F. The autocorrelation timescale for atmospheric disturbances is of the order of 10 days (Lorenz 1973). We have chosen τ_F to be 30 days. Since we are interested in the variability around the mean state in Fig. 3, we want the stochastic component of the freshwater flux to be a relatively small perturbation. Thus, we have chosen the standard deviation of the stochastic forcing, $\langle S^2 \rangle^{1/2}$ equal to 20% of the maximum value of the mean $E - P$ field in Fig. 2. This is similar to the approach of Mikolajewicz and Maier-Reimer (1990) in their stochastically forced experiments. Statistics of the $E - P$ field for the period 1979–1995 have been computed by Trenberth and Guillemot (1996) from the reanalysis maps produced at the National Centers for Environmental Prediction. In high northern latitudes, where precipitation exceeds evaporation, the annual mean standard deviation is about 25%–30% of the annual mean $E - P$. Thus, our choice for the amplitude of the stochastic forcing is not very different from the results of Trenberth and Guillemot.

We are interested in exploring the sensitivity of the variability to different choices for the spatial pattern of the stochastic forcing. In particular, the question we want to answer with this analysis is whether different modes of variability emerge with different distributions of the surface random component or whether there is just one mode of variability that can be excited, independent of spatial pattern. In the latter case different patterns may have different degrees of coupling with the oceanic mode and be more or less efficient in exciting it. Thus, the amplitude of the response as a function of the spatial distribution of the random forcing can give some indications about the nature of the oceanic mode and of its underlying dynamics. If, on the other hand, preferred timescales originate from oceanic advection through areas of coherent atmospheric forcing, spatial patterns with different characteristic spatial scales should give rise to different dominant timescales.

The first two choices for the spatial pattern consist in choosing just one wavenumber (the first) in the zonal and meridional directions, respectively. The random forcing is applied only in the Northern Hemisphere so that wavenumber 1 corresponds to wavelengths of 60° in the zonal direction and 69° in the meridional direction. The resulting spatial patterns are shown in Fig. 4 (two left panels). In the case of spatial pattern 1 the amplitude of the stochastic forcing is also modulated in the meridional direction with a hyperbolic tangent function whose values increase from zero at the equator to unity approaching the northern boundary.

These two cases are intended to test the effect of an east–west density gradient induced by the random forcing versus a north–south gradient. We then investigate the effect of reducing the spatial scale of the forcing by considering wavenumber 3 distributions in both the zonal (wavelength of 19.7°) and meridional (wavelength of 23°) directions (Fig. 4, right panel). In all cases, the horizontal average of these patterns is identically zero; no net freshwater is added by the random processes.

It is important to emphasize that the choice of stochastic forcing is not intended to reproduce aspects of the real atmospheric forcing. The first issue we want to address is, in fact, simply related to the identification of the possible modes of variability of the ocean model. Their emergence may be a function of the particular spatial pattern that is chosen. As a second step one may want to ask the question of whether realistic atmospheric forcing can excite the mode (or modes) that the ocean model supports. This second question will be addressed in the more realistic context of the North Atlantic model.

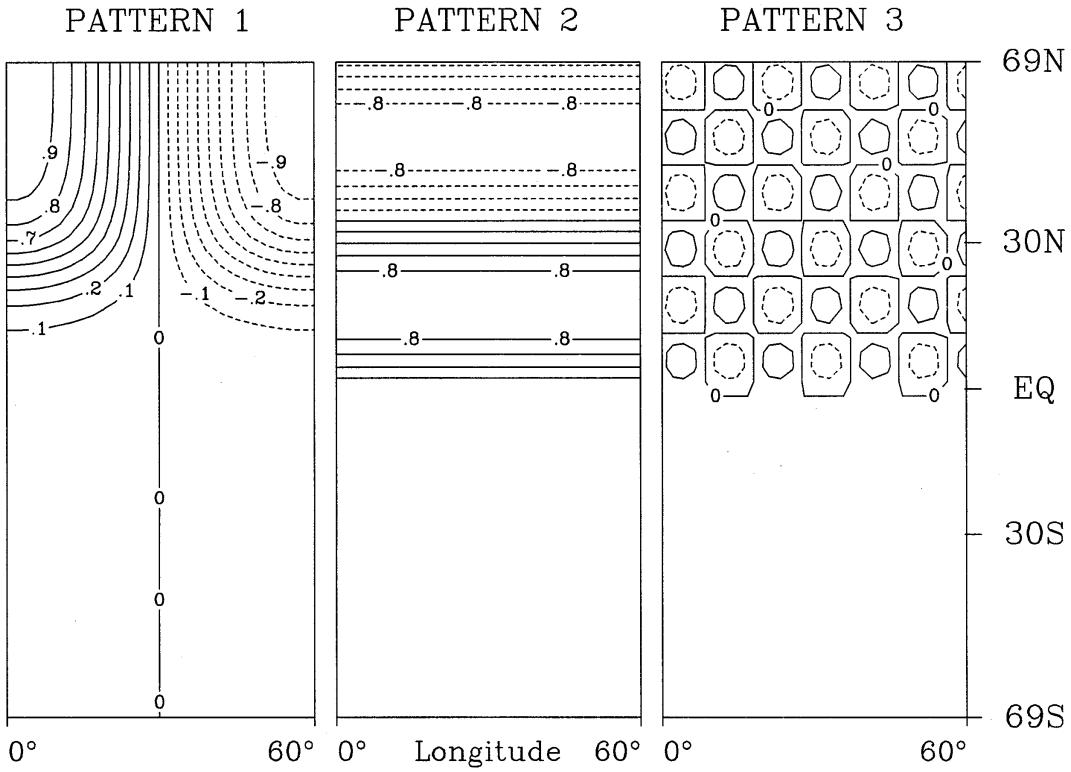

FIG. 4. Spatial patterns of the stochastic component of the freshwater flux. The stochastic forcing is applied only in the Northern Hemisphere. Spatial pattern 1 is chosen as a dipole in the east–west direction, spatial pattern 2 is prescribed as a sine function in the meridional direction (wavelength of 69°), and spatial pattern 3 is defined as the product of two sine functions in both the zonal and meridional directions (wavelengths of 19.7° and 23°, respectively).

b. Thermal boundary conditions

The surface thermal boundary conditions that have been traditionally used in ocean only simulations are restoring boundary conditions: the surface heat flux is estimated by relaxing the model SST T_S toward a prescribed temperature distribution T^*

$$Q = -c(T_S - T^*). \tag{8}$$

The coupling constant c is of the order of 40 W m^{-2} K^{-1}, leading to restoring timescales of 30–60 days for typical mixed layer depths. This formulation for the surface heat flux is based on the work of Haney (1971) and is derived by considering local air–sea interactions and assuming an unchangeable atmosphere, an atmosphere with an infinite heat capacity. On the contrary, the atmospheric heat capacity is much smaller than the oceanic one, leading to atmospheric timescales that are much faster than the oceanic timescales. As a result, one may expect that localized SST anomalies might determine a relatively fast readjustment of the atmosphere so that the ocean–atmosphere heat exchange at any given point depends upon the global atmospheric state (Bretherton 1982). In particular, different atmospheric processes can be expected to be responsible for the dissipation of SST anomalies of different spatial scales: SST anomalies of some hundreds of kilometers, for example, can be expected to be dissipated by winds, a relatively efficient and fast process, while global scale anomalies can only be dissipated through radiation to space, a much more inefficient and slow process. Thus, the lifetime of SST anomalies can be expected to be scale dependent.

Recent studies (Zhang et al. 1993; Rahmstorf and Willebrand 1995) have tried to incorporate the effects of an interactive atmosphere in the formulation of the surface thermal boundary conditions. They have adopted energy-balance-type models for the atmosphere with either fixed (Zhang et al. 1993) or diffusive (Rahmstorf and Willebrand 1995) meridional heat transport. In the case of a fixed heat transport the resulting thermal boundary condition can still be expressed in the form of a Newtonian relaxation law, but the restoring constant c is about one order of magnitude smaller than the one from Haney's formulation. In the following we will refer to this boundary condition as EB0. In the diffusive atmospheric transport case, on the other hand, the resulting boundary condition takes the form

$$Q = -c(T_S - T^*) + \mu\nabla^2(T_S - T^*). \tag{9}$$

The surface heat flux now contains two terms: the first term has the form of a weak restoring as in the fixed transport case (with the constant c much smaller than

TABLE 1. List of the different thermal boundary conditions considered in this study.

Boundary condition	c (W m^{-2} K^{-1})	τ (days)	μ (W K^{-1})	Description
RST1	232	6		Restoring
RST2	46	30		Restoring
RST3	23	60		Restoring
RST4	12	120		Restoring
EB0	2.3	600		Restoring
EB1	2.3		10^{13}	Rahmstorf and Willebrand (1995)
FBC				Flux

in Haney's restoring), expressing the slow damping of SST anomalies through radiation to space. The second term in (9) introduces a scale dependence in the surface heat flux, thus accounting for the more efficient damping of SST anomalies by atmospheric transport processes at spatial scales smaller than the global one. This boundary condition will be referred to as EB1.

It has been shown (Zhang et al. 1993; Rahmstorf and Willebrand 1995) that the ''alternative'' boundary conditions EB0 and EB1 enhance the stability of the meridional overturning and prevent the occurrence of catastrophic instabilities such as the ''polar halocline catastrophy'' mentioned above. Capotondi and Saravanan (1996) have shown that the diffusive assumption for the atmospheric transport as in Rahmstorf and Willebrand (1995) can mimic quite well some of the atmospheric feedbacks found in an idealized coupled ocean–atmosphere model (Saravanan and McWilliams 1995), feedbacks associated with the atmospheric meridional transport processes. However, the accuracy of the EB boundary conditions in more realistic three-dimensional scenarios has not yet been tested.

We consider here a sequence of thermal boundary conditions. They include restoring boundary conditions with different restoring timescales, ranging from values typical of a Haney-type approach (''strong'' restoring cases) to values more appropriate to the energy balance formulation. We also consider the boundary condition proposed by Rahmstorf and Willebrand (1995) [Eq. (9)] as well as a fixed flux boundary condition. The complete list of boundary conditions is summarized in Table 1. In this table the boundary conditions described as ''restoring'' refer to expression (8). In this case τ is the corresponding damping timescale. The boundary condition described as ''Rahmstorf and Willebrand'' is the one defined in Eq. (9). The value of the constant c has been chosen equal to the one used for EB0. Our choice for the constant μ leads to a heat flux sensitivity (variation produced in the heat flux by a SST anomaly of unit value) of 12.3 W m^{-2} K^{-1} for anomalies of 1000-km scale. This is very similar to the value used by Rahmstorf and Willebrand (1995), whose choice for the heat flux sensitivity at the same scale was 11 W m^{-2} K^{-1}. In both cases the value of the heat flux sensitivity lies in the range of 10–30 W m^{-2} K^{-1}, which has been estimated to correspond to realistic lifetimes of SST anomalies at 1000-km scale (Anderson and Willebrand 1992). Notice that at these scales the heat flux sensitivity for the EB1 boundary condition is very similar to the one for RST4 so that at these scales the two boundary conditions can be expected to have a similar behavior. At spatial scales larger than 1000 km EB1 will tend to approach EB0, while at smaller scales EB1 will damp SST anomalies much faster.

The dynamical consequences of the different boundary conditions in Table 1 are in the degree to which they allow the manifestation of the negative temperature feedback at high latitudes (see Willebrand 1993 for a discussion of the feedbacks of the ocean thermohaline circulation). If the meridional overturning weakens, for example, the northward heat transport is reduced. The resulting colder temperatures have the effect of increasing the density and therefore stabilizing the thermohaline circulation (a negative feedback). In the strong restoring cases, however, the SST is forced to remain very close to the prescribed field T^*, thus reducing or inhibiting the possibility of this temperature feedback. Only in the case of weak restoring or flux boundary condition does the model SST have some freedom to respond to changes in the ocean circulation. The extreme case is the flux boundary condition that leaves the SST completely free to evolve. The sensitivity of the model variability to the specification of the different boundary conditions is therefore an indication of the relevance of the negative temperature feedback to the dynamics of the variability itself.

We are interested in the model variability around the reference state in Fig. 3. Thus, in the implementation of the different boundary conditions we require that they be in equilibrium with this state. In the case of the restoring and EB1 boundary conditions this is achieved by solving Eqs. (8) and (9) for T^*, given c, Q, and T_S. In the flux boundary condition case the equilibrium heat flux Q (as diagnosed from the restoring term of the spinup experiment) is used. In all cases the model has been run for several hundred years to ensure that a complete adjustment to the different boundary conditions is achieved before starting the stochastically forced experiments.

3. The stochastically forced experiments

We first consider the simulations performed with spatial pattern 1 in Fig. 4 and compare the results obtained

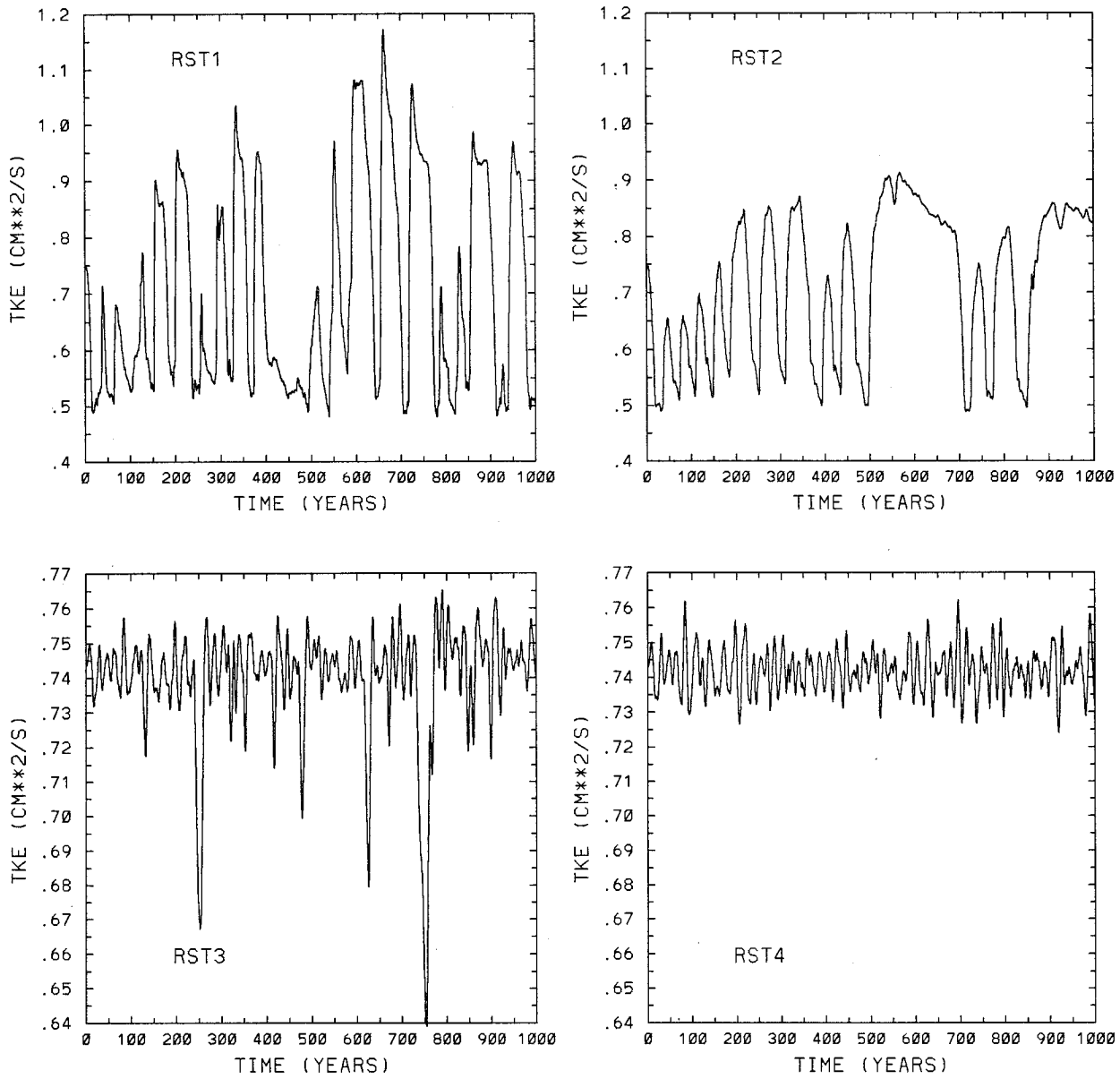

FIG. 5. Time evolution of globally averaged total kinetic energy for boundary conditions RST1 (τ = 6 days), RST2 (τ = 30 days), RST3 (τ = 60 days), and RST4 (τ = 120 days).

with the different thermal boundary conditions. We will find that the characteristics of the variability in the various cases are very similar as long as the SST has some freedom to respond to changes in the circulation. The consequences of using different spatial patterns are then investigated only in the case of the flux boundary condition.

All simulations have been carried out for 1000 years. Figure 5 shows time series of globally averaged total kinetic energy for RST1, RST2, RST3, and RST4 over the total duration of the simulation. In the first two cases large and irregular variations in total kinetic energy are found. In the case of RST3 (restoring timescale of 60 days) periods of smaller amplitude oscillations alternate with events of very low total kinetic energy. Finally, when a restoring timescale of 120 days is used, more ''regular'' oscillations are found. Given the freshwater flux forcing chosen for these experiments, a restoring timescale of 60 days appears to be the transition value between the oscillatory behavior found with RST4 and the large excursions in total kinetic energy observed with RST1 and RST2. The associated spectra (Fig. 6) show the tendency to integrate the white noise signal (displayed in the top-left panel), as one can expect from the ocean tendency to remove very fast timescales. However, it is only in the case of RST4 that a spectral

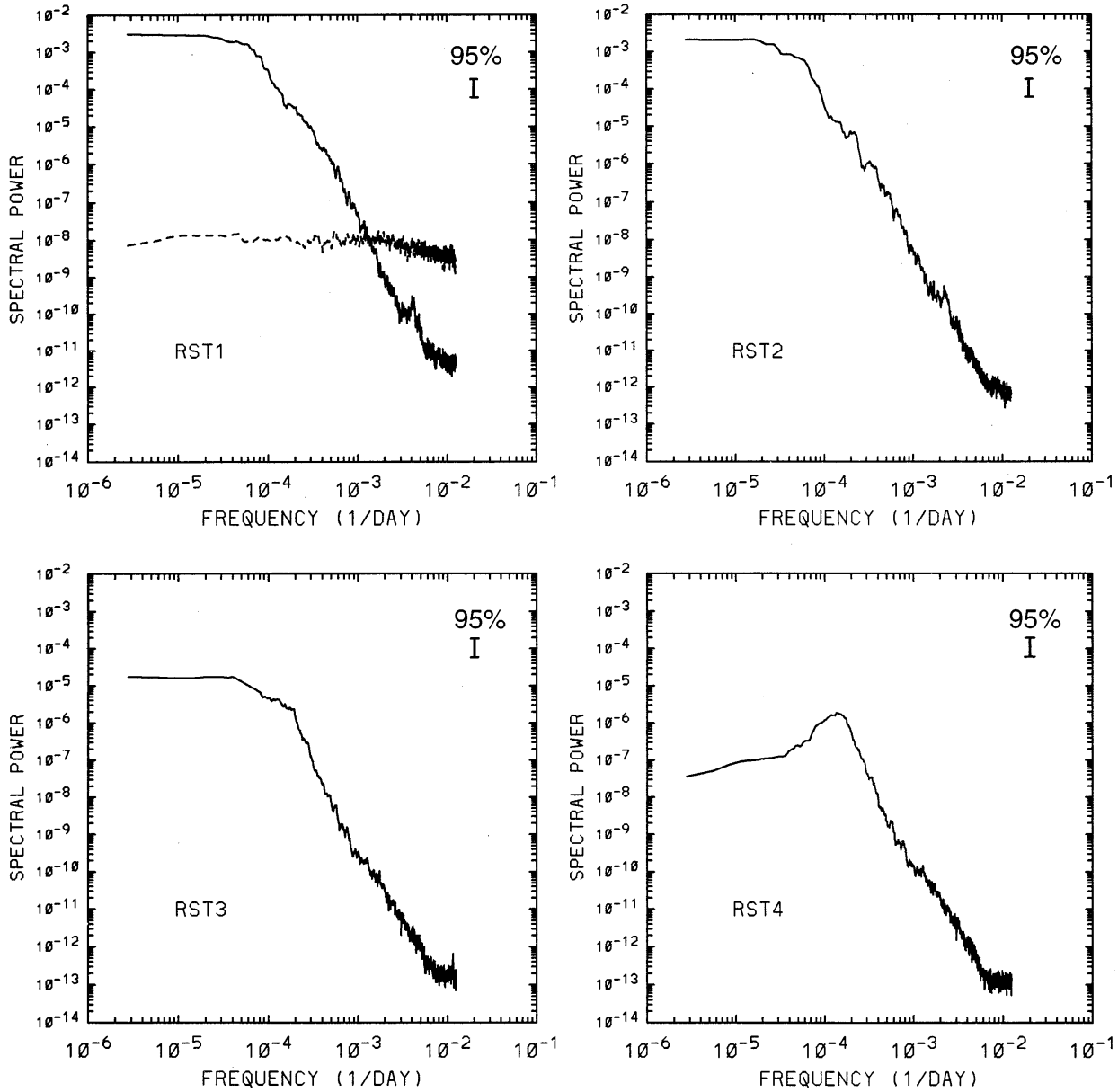

FIG. 6. Frequency spectra for the time series shown in Fig. 5. In the top-left panel the spectrum of the random component of the freshwater flux (dashed line) is also shown for comparison.

peak (at approximately 24 yr) appears. The remaining boundary conditions (EB0, EB1, FBC) produce results very similar to RST4. The four spectra (RST4, EB0, EB1, FBC) are compared in Fig. 7.

In the four latter cases a spectral peak emerges at approximately the same frequency. Notice that the position and amplitude of the peak for FBC are very similar to the ones for EB0. The same is true for RST4 and EB1. This seems to suggest that the amplitude of the variability increases with increasing intensity of the negative temperature feedback. Thus, the boundary conditions that constrain the SST the least (EB0 and FBC) give rise to the most pronounced peaks. In the following we first investigate the nature of the large excursions in total kinetic energy that are observed with RST1, RST2, and RST3. Then we analyze and compare the characteristics of the variability that is found with EB0, EB1, and FBC (weak SST constraint).

a. Strong restoring cases

In order to understand the nature of the irregular variations in total kinetic energy that are observed with strong restoring (RST1 and RST2) in Fig. 5, we have considered composites of meridional overturning for high (larger than 0.75 $cm^2\ s^{-1}$) and low (smaller than

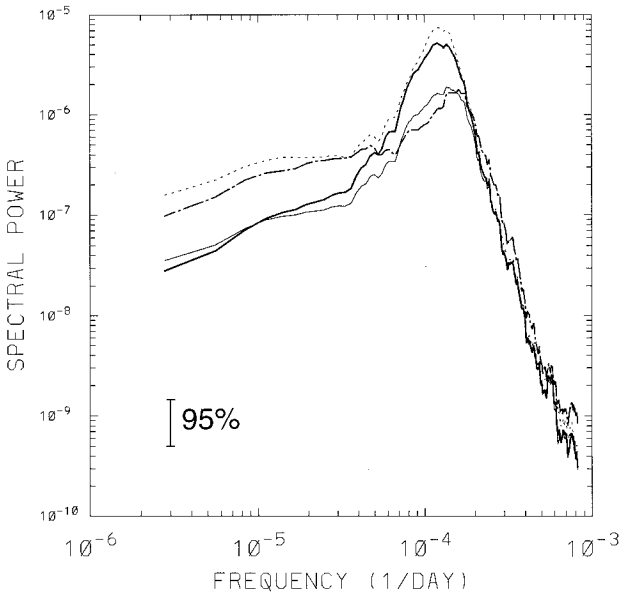

FIG. 7. Spectra of the total kinetic energy time series obtained with RST4 (thin solid line), EB0 (thick solid line), EB1 (thick dot–dashed line), and FBC (thin dotted line).

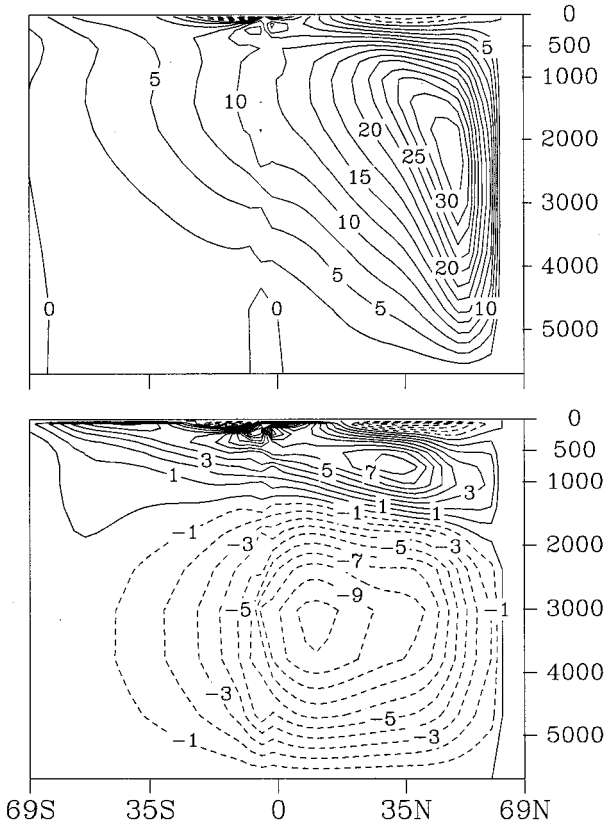

FIG. 8. Composites of meridional overturning for high (top) and low (bottom) total kinetic energy levels in the case of RST2. Contour interval is 0.5 Sv for the top panel and 1 Sv for the bottom panel.

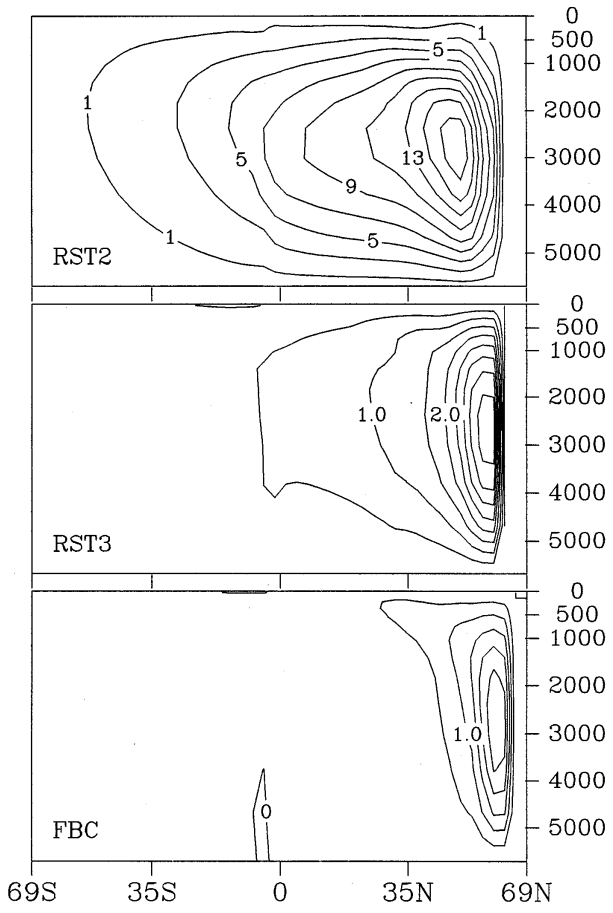

FIG. 9. EOF1 of meridional overturning for RST2 (top, contour interval 2 Sv), RST3 (middle, contour interval 0.5 Sv), FBC (bottom, contour interval 0.5 Sv).

0.55 cm^2 s^{-1}) total kinetic energy levels, respectively. They are shown in Fig. 8. The case we concentrate upon is RST2. The different total kinetic energy levels correspond to dramatic variations in the intensity of the meridional overturning going from a very energetic overturning (Fig. 8, top) to an almost collapsed state (Fig. 8, bottom).

An empirical orthogonal function (EOF) analysis shows that about 90% of the variance in the meridional overturning in the RST2 case is accounted for by the first EOF (Fig. 9, top). The associated variability consists in a vigorous overturning cell reaching south of the equator. The large changes in the intensity of the meridional overturning lead to variations as large as 70% in the maximum northward heat transport (Fig. 10, top left). The evolution of the surface oceanic heat flux (Fig. 11) shows dramatic variations between periods of almost vanishing heat loss and sudden episodes of very large heat loss. This behavior is characteristic of ''flush type'' variability as extensively described by other authors (Marotzke 1989; Weaver and Sarachik 1991; Weaver et al. 1993; Chen and Ghil 1995). Flushes result

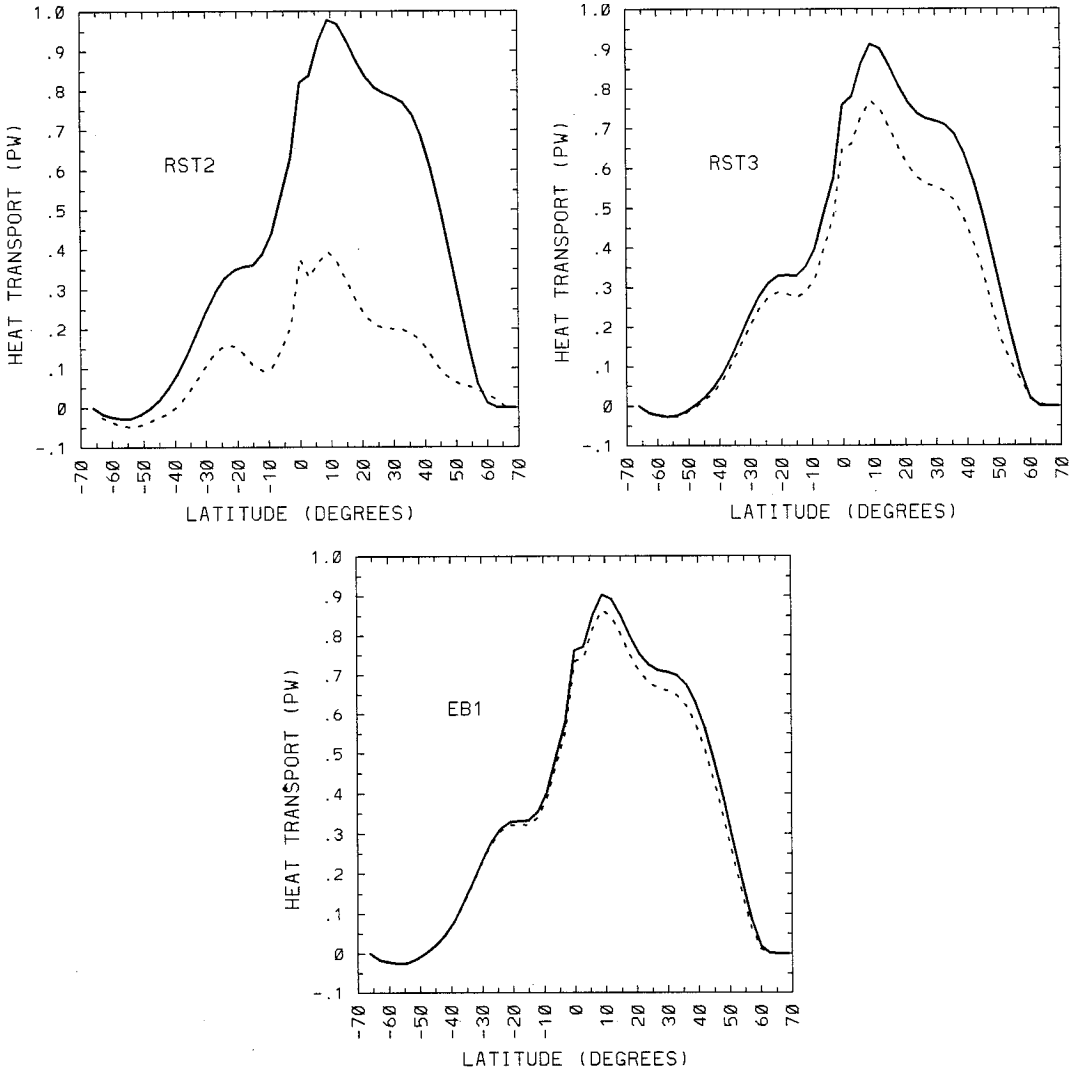

FIG. 10. Composites of northward heat transport (in PW) for strong overturning (solid line) and weak overturning (dashed line) in the cases of RST2 (top left), RST3 (top right), and EB1 (bottom). Strong overturning events and weak overturning events are defined by values of total kinetic energy larger than a given threshold (0.755 $cm^2\ s^{-1}$ for RST2 and RST3, and 0.75 $cm^2\ s^{-1}$ for EB1) and smaller than a given threshold (0.55 $cm^2\ s^{-1}$ for RST2, 0.68 $cm^2\ s^{-1}$ for RST3, and 0.735 $cm^2\ s^{-1}$ for EB1), respectively.

from the diffusive warming of the subsurface model layers during phases of very weak overturning and consequent establishment of statically unstable conditions leading to very strong overturning. The timescale of vertical diffusion over a 1000-m depth is of the order of a few hundred years. In most of the previous studies flushes were, in fact, observed at regular intervals of some hundred years. The presence of the stochastic forcing in this simulation affects both the timescale and the amplitude of the flushing events. Their occurrence is irregular and more frequent and their amplitude can vary considerably from one episode to another. This is consistent with the results of Weaver et al. (1993) who found that the inclusion of a relatively large stochastic component in the surface freshwater flux had the effect of reducing the amplitude of the flushes and increasing their frequency. An EOF analysis of the surface temperature fields for the RST2 case (not shown) shows that 8% of the variance (EOF3) is accounted for by an oscillatory signal with a period of 40–50 years, which approximately corresponds to the frequency of the flushes during the periods 0–500 years and 700–800 years in Fig. 5.

From this analysis we can conclude that the dominant signal that is found with strong restoring boundary conditions is a flush-type variability. Weaver et al. (1993) have shown that decadal variability can occur in ocean models whose surface temperatures are restored with a timescale comparable to RST2, while flushes were observed in experiments in which the model SST were much more weakly constrained (Weaver and Hughes 1994). For a given thermal coupling constant the type

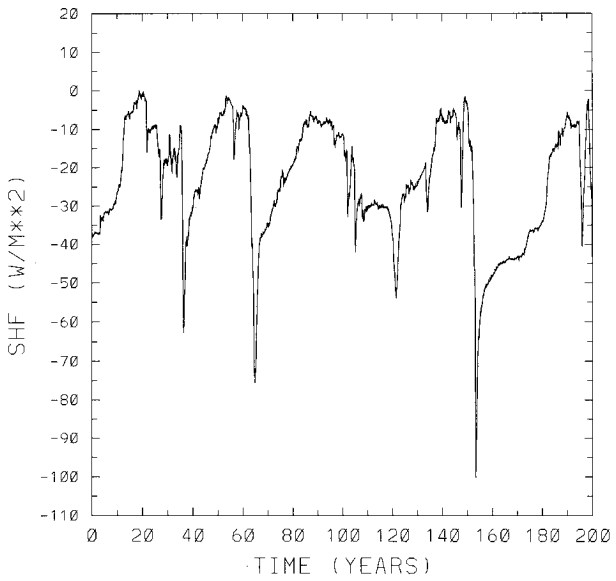

FIG. 11. Variation of the surface heat flux averaged over the western half of the Northern Hemisphere for case RST2.

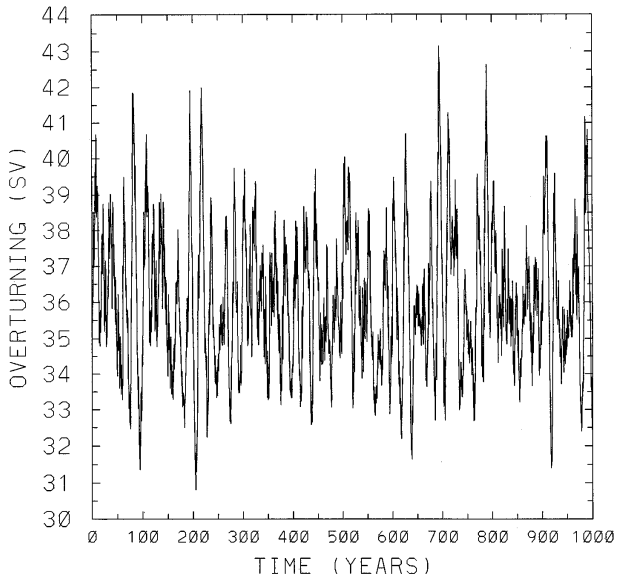

FIG. 12. Evolution of the strength of the meridional overturning (in Sv) for the case FBC.

of variability exhibited by the model is dependent upon the relative strength of haline versus thermal forcing. The larger the freshwater flux into the ocean at northern high latitudes, the larger temperature variations need to be in order to counteract the destabilizing salinity effects. Therefore our definition of ''strong restoring'' is relative to the particular freshwater forcing (mean plus variability) chosen for our experiments.

In the case of RST3 the variability of the meridional overturning, as described by EOF analysis, is much smaller and more confined to the Northern Hemisphere (Fig. 9, middle). Consequently, the variations in the northern heat transport are largely reduced (Fig. 10, top right). The variance of the total kinetic energy in this case is dominated by the isolated events of large energy decrease. The corresponding spectrum in Fig. 6 is red. However, EOF analysis of the temperature fields is able to isolate the intermittent oscillatory behavior at decadal timescale that can be observed in Fig. 5. In fact, the time series of EOF4 shows a peak at 20–25 years (not shown). The fraction of the variance accounted for by the decadal mode is 5% in this case.

b. Weak SST constraint

We have seen in the previous sections that the possibility for the SST to respond to changes in the circulation leads to an oscillatory model behavior associated with the appearance of a peak in the spectrum of some of the model variables. We now analyze in more detail the characteristics of this oscillatory behavior in the various cases. We will concentrate on the EB0, EB1, and FBC boundary conditions. An empirical orthogonal function approach is used to reduce the number of degrees of freedom.

Figure 12 shows the variation of the strength of the meridional overturning over the duration of the integration for the FBC case. The deviations from the mean value are of the order of 15%–17%. Similar results are obtained for EB0 and EB1. In all three cases the meridional overturning variability is mainly described by the first EOF, which accounts for about 80% of the variance. The associated signal is concentrated in the area north of approximately 40°N, as can be seen in Fig. 9 (bottom panel) for the FBC case. Similar results are also obtained for the other two boundary conditions (not shown). The time variation of the first EOF is also similar in all three cases. The corresponding spectra (Fig. 13) show a peak at the decadal timescale and a bulge at lower frequencies. The main difference is in the intensity of the decadal peak, which appears more pronounced in the case of the flux boundary condition than in the other two cases. As remarked for the total kinetic energy spectra (Fig. 7), the intensity of the decadal peak appears to increase with decreasing SST constraint; the freer the SST to respond to changes in the circulation (and therefore the larger the negative temperature feedback), the larger the response at decadal timescales.

Notice how the meridional streamfunction variability varies from the large basin-scale signal obtained in the case of RST1 and RST2 (Fig. 9, top) to a smaller amplitude signal limited to an area close to the northern boundary in the weak restoring cases (Fig. 9, bottom). Consequently, in the weak restoring cases the northward heat transport does not vary appreciably between the phases of stronger and weaker overturning as can be seen in Fig. 10 (bottom) for the EB1 case. The structure of meridional overturning EOF1 for the weak restoring cases (Fig. 9, bottom) is very similar to the one found by Saravanan and McWilliams (1996a) in an idealized

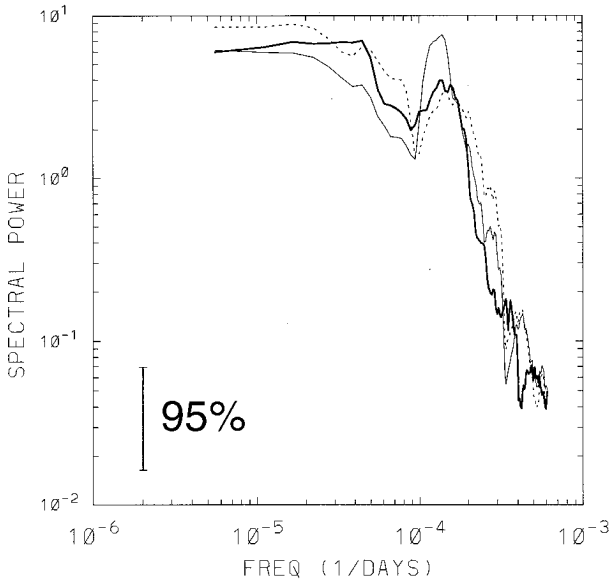

FIG. 13. Spectra of the time series of the meridional overturning first EOF in the case of FBC (thin solid line), EB0 (thick solid line), and EB1 (thin dashed line).

coupled ocean–atmosphere model. It seems to indicate that variability at decadal timescales arises from processes (perhaps advection of temperature and/or salinity anomalies) confined to northern high latitudes in the spirit of that described by Weaver and Sarachik (1991).

Since the temperature feedback seems to play a crucial role in the establishment of an oscillatory behavior at decadal timescales, the variability occurring in the temperature field is of particular interest. Such variability is mainly concentrated in the Northern Hemisphere. Thus, we use only Northern Hemisphere values for the EOF analysis. We consider three vertical levels: the surface, level 8, and level 13. Level 8 is at approximately 1000 m, within the northward flowing branch of the model conveyor belt (Fig. 3), while level 13 is at approximately 3500 m, within the southward return flow of the meridional overturning.

SST anomalies associated with the first three EOFs for the three boundary conditions are compared in Fig. 14, and the corresponding spectra are shown in Fig. 15. The mean velocities for the various cases are also included for comparison. In all cases, the first three EOFs account for about 85% of the variance, with EOF1 accounting for about 50%, EOF2 for about 20%, and EOF3 for approximately 10%. The EOF patterns for the different boundary conditions have very strong similarities, especially the ones associated with FBC and EB0. The EOFs obtained with EB1 have a smoother aspect, probably due to the diffusive term of this boundary condition. EOF1 exhibits a major center of action around 30°N, close to the eastern boundary, which corresponds to a region of mean flow convergence. A weaker center of opposite polarity is located at about 50°N close to the western boundary. This is approximately the location where the mean western boundary current separates from the coast. The latter is also the area where EOF2 reaches the largest amplitude, with a weaker center of action of opposite sign centered at about 30°N toward the southeast. The pattern of EOF3 is somewhat noisier in the cases of FBC and EB0. The major centers of action remain the one at about 30°N close to the eastern boundary and the one around 50°N close to the western boundary. The corresponding spectra (Fig. 15) show that EOF1 is basically associated with a red spectrum, while EOF2 captures the decadal mode. EOF3 also shows a peak at decadal timescales in the case of FBC, but the spectrum is essentially white in the other two cases at low frequencies.

These results are reminiscent of the findings of Deser and Blackmon (1993) in their analysis of 90 winters of SST data from the Comprehensive Ocean–Atmosphere Data Set (COADS). They found that the first SST EOF accounted for 45% of the variance and was characterized by a red spectrum reflecting the transition from below-normal SST values to above-normal SST values. The second EOF, which accounted for 12% of the variance, exhibited quasi-biennial as well as quasi-decadal oscillations. The dipolelike structure of EOF2 in Deser and Blackmon's (1993) results has also some similarities with the pattern of EOF2 in our results. However, EOF1 is very different. In their case the major center of action is located along the axis of the separated Gulf Stream, close to the western boundary, while in our case the largest amplitude is found close to the eastern boundary.

Although the decadal signal seems to dominate integral quantities such as the total kinetic energy and to some extent the meridional overturning, it only accounts for a fraction of the temperature variance. The larger fraction of the temperature variance (EOF1) reflects the local effect of the surface stochastic forcing; the white noise signal is integrated by the ocean model to a red spectrum as described by Hasselman (1976). However, there is also a ''nonlocal'' effect involving the ocean dynamics (either by exciting a mode of variability of the ocean model or as a result of oceanic advection through the area of stochastic forcing), which results in the emergence of a spectral peak. Both effects are present in the variability of the temperature field, but only the second one appears in the variability of integral quantities such as the total kinetic energy.

The maximum amplitude of temperature EOF2 is about 0.3°C. Observational estimates of temperature anomalies at decadal timescale range from about 0.3°C for annual mean values (Saravanan and McWilliams 1996b) to about 1.5°C for winter conditions (Deser and Blackmon 1993). Therefore our results, which can be considered representative of annual mean values, are consistent with observational estimates.

The depth dependence of the anomalies is illustrated in Fig. 16 for the FBC boundary condition. Notice the strong correspondence between the major centers of ac-

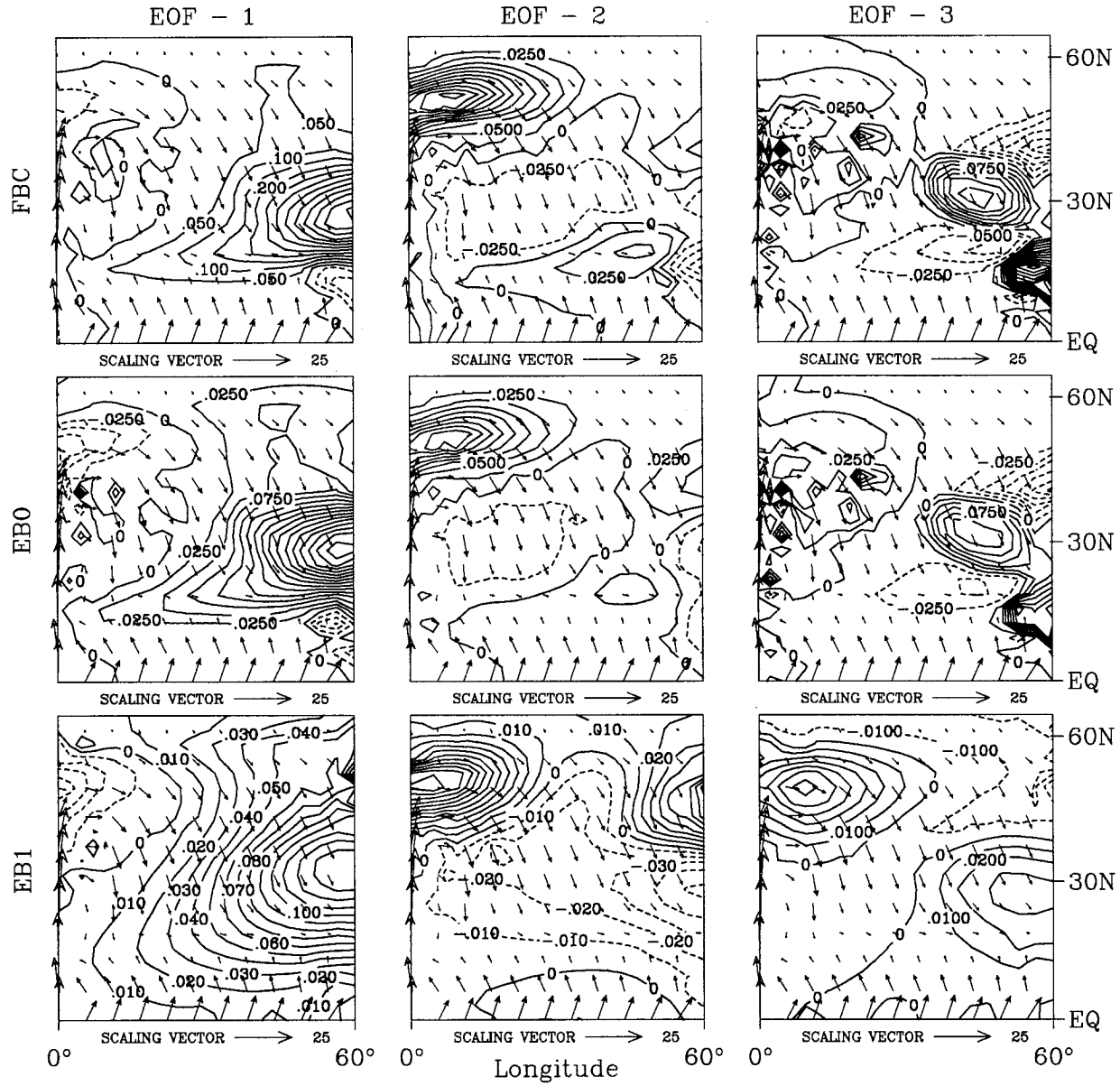

FIG. 14. EOFs of SST for boundary conditions FBC (top), EB0 (middle), and EB1 (bottom). Values are in °C. EOF1 (left) accounts for 52% of the variance in the FBC case, 45% in the EB0 case, and 47% in the EB1 case. EOF2 (middle columnn) accounts for 18% of the variance for FBC, as well as for EB0 and EB1. EOF3 (right columnn) accounts for 10% of the variance for FBC, 12% for EB0, and 9% for EB1. Mean velocities (in cm s^{-1}) are also plotted for comparison. Only the northern half of the basin is shown.

tion of the EOFs at the different levels and the position of the most intense components of the mean circulation at the same levels. In particular, at level 13 temperature anomalies are mainly concentrated along the northern boundary where the deep branch of the model conveyor belt flows.

The first salinity EOF (not shown) is dominated by an east–west dipole structure in the first level, clearly attributable to the spatial pattern of the stochastic forcing. The corresponding spectrum is white at periods longer than approximately 10 years. None of the higher-order EOFs captures the decadal mode as for temperature, their spectra being essentially red.

The previous analysis shows that when the model SST is not strongly constrained by the surface thermal boundary conditions variability at a decadal timescale can occur, and the characteristics of this variability are qualitatively very similar in the various cases. However, there seems to be an indication that the larger the temperature variations allowed by the surface thermal boundary condition, the more pronounced the oscillation. This result seems to be in agreement with the re-

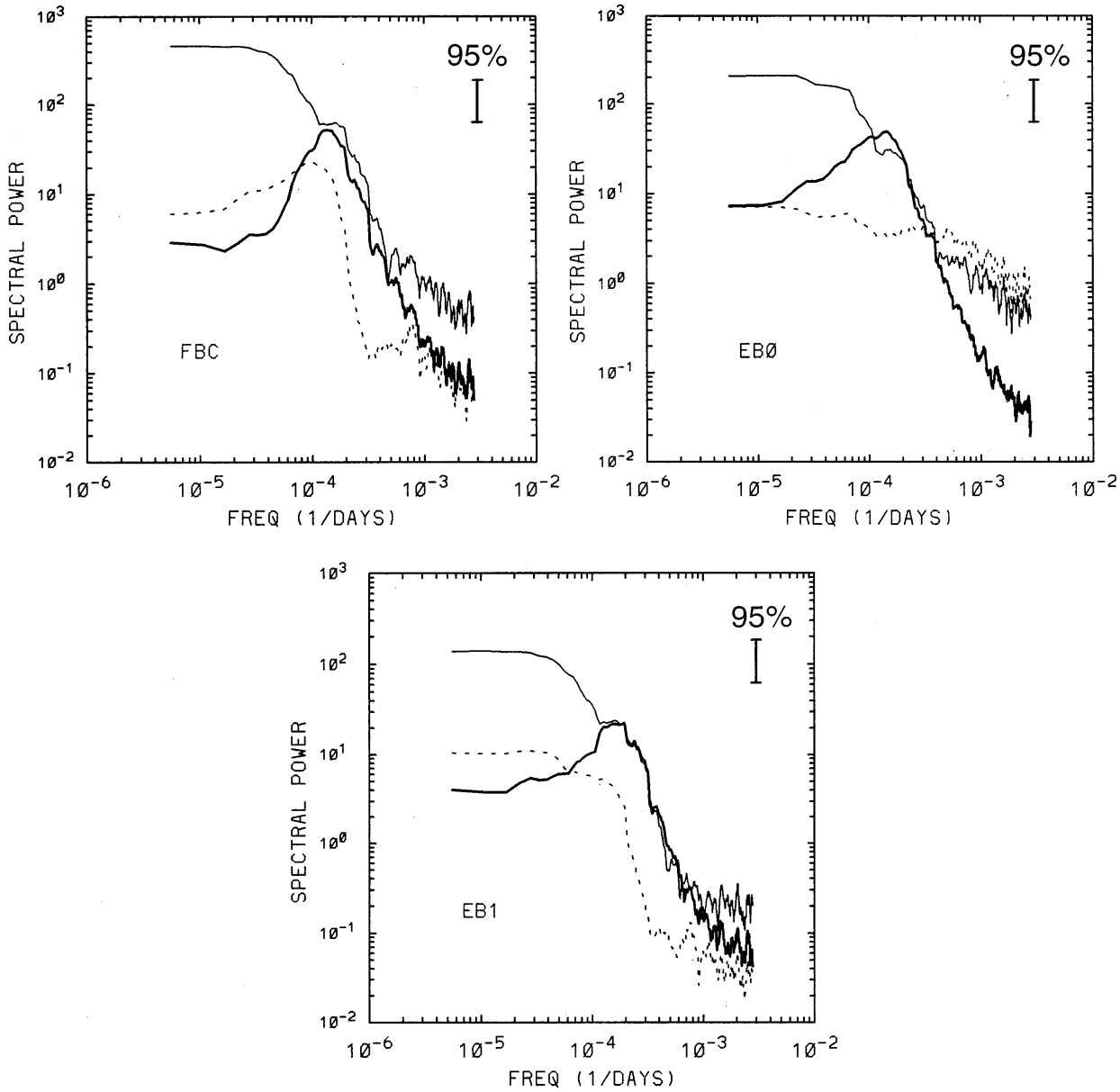

FIG. 15. Spectra of time series of EOF1 (thin solid line), EOF2 (thick solid line), and EOF3 (thin dashed line), in the case of FBC (top left), EB0 (top left), and EB1 (bottom) boundary conditions. The spectra have been normalized so that the area is proportional to the variance accounted for by the corresponding EOF.

sults of Greatbatch and Zhang (1995) who found a self-sustained oscillation in a model driven only by constant surface heat flux (the salinity was held constant in the model).

c. Sensitivity to the spatial pattern

Two additional experiments with spatial patterns 2 and 3 (see Fig. 4) have been performed using the FBC boundary condition. To have an appreciable ocean model response the amplitude of the stochastic forcing was doubled in the case of spatial pattern 3. The basic aspects we are interested in investigating are associated with the possible dependence of the dominant frequency of the variability, or of its amplitude, upon the spatial structure of the forcing. Spectra of total kinetic energy (averaged over the whole domain) and meridional overturning for the three spatial patterns are shown in Fig. 17. In all three cases the frequency of the spectral peak is approximately the same. The characteristic spatial scale of the forcing does not affect the dominant timescale of the variability, thus ruling out the mechanism proposed by Saravanan and McWilliams (1996b) for setting the timescale. The decadal variability found in

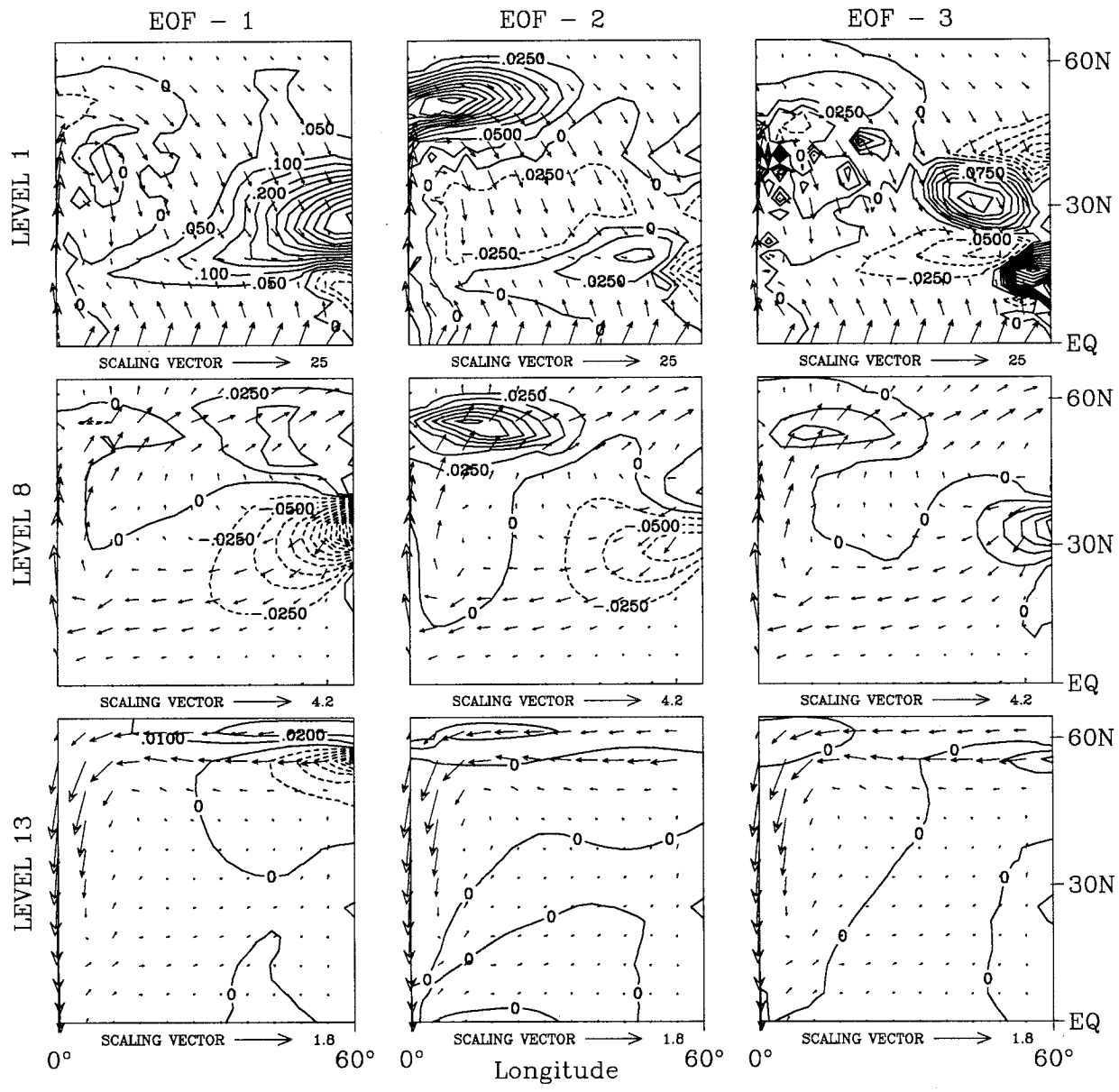

FIG. 16. Temperature EOFs for the FBC boundary conditions at level 1 (top row), level 8 (middle row), and level 13 (bottom row). EOF1 accounts for 52% of the variance, EOF2 for 18%, and EOF3 for 10%. Mean velocities (in cm s^{-1}) in the various levels are also shown for comparison.

this model appears to be associated with an oscillatory mode of the ocean model more in agreement with the scenario proposed by Griffies and Tziperman (1995). However, a secondary peak at about 450-day period can be observed in the spectrum of the total kinetic energy for spatial pattern 3. A timescale of 450 days is the one that can be derived following Saravanan and McWilliams' (1996b) argument by considering the wavelength of spatial pattern 3 (about 2000 km) and the mean velocity of the western boundary current over the top 1000 m (about 6 cm s^{-1}). The depth of 1000 m corresponds, from Fig. 3, to the northward flowing branch of the model conveyor belt. Thus, it is possible that the mechanism proposed by Saravanan and McWilliams (1996b) plays some role in these simulations, but it is a secondary role compared to the intrinsic ocean model variability.

Although the spatial pattern of the forcing does not seem to affect the dominant frequency of the variability, it does affect the amplitude of the response. Different spatial patterns have different degrees of efficiency in exciting the decadal mode. A north–south gradient in the surface freshwater forcing (spatial pattern 2) seems to produce a large variance in the oceanic response, but

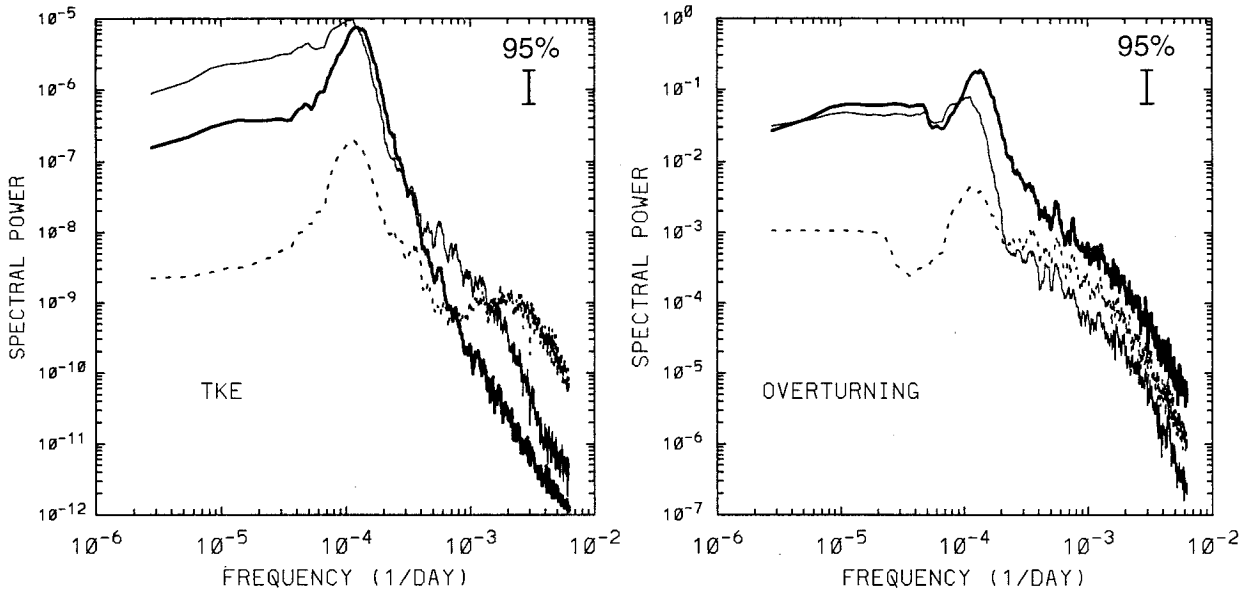

FIG. 17. Frequency spectra of total kinetic energy time series (left) and meridional overturning (right) for different spatial patterns of stochastic forcing: spatial pattern 1 (thick solid line), spatial pattern 2 (thin solid line), and spatial pattern 3 (dashed line).

a relatively weaker decadal signal above the background. The EOF analysis of the temperature fields shows that the EOF associated with the decadal mode accounts for only 12% of the variance in this case (versus the 18% in the case of spatial pattern 1). Therefore, the east–west dipole in the forcing seems to be more effective in exciting the decadal signal than the north–south dipole as one would intuitively expect. In fact, for spatial pattern 1 the surface forcing directly affects the east–west density difference, which ultimately drives the meridional overturning.

The decrease in the spatial scale of the forcing (spatial pattern 3) results in a much weaker (almost two orders of magnitude) decadal peak in spite of the larger amplitude of the forcing. The decadal signal is absent in the time series of temperature and salinity EOFs, whose spectra are essentially white.

The main conclusion of this section is that the variability at 20–25 years is associated with an oscillatory mode of the ocean model, which appears to be the only mode excited in the present modeling scenario. Large-scale forcing, especially if acting on the east–west density gradient, is much more efficient in exciting the oceanic mode than small-scale forcing.

d. Thermal stochastic forcing

In this section we verify that adding a stochastic component to the surface heat flux results in a model response similar to the one obtained with stochastic forcing in the freshwater flux. For this purpose we consider the FBC case and spatial pattern 1. The amplitude of the random forcing is chosen so that the resulting density variations are, on average, equivalent to the variations produced by the random forcing in the freshwater flux. The model response obtained in this case is indeed very similar to the FBC experiment with stochastic freshwater forcing. The spectra of total kinetic energy and meridional overturning (Fig. 18) are almost indistinguishable in the two cases. However, one may wonder what the effect of a random component in the surface heat flux upon the variability in the temperature fields themselves may be.

EOF analysis (Fig. 19) of the temperature fields results in a dominant EOF accounting for 69% of the variance, whose east–west dipole structure is clearly associated with the stochastic forcing. Thus, when white noise is added to the surface heat flux, a larger fraction of the variance in the temperature field is associated with the oceanic integration of the white noise forcing. However, EOF2 (which accounts for 10% of the variance) is associated with the decadal mode and is very similar to the corresponding EOF in the freshwater flux driven case (Figs. 14 and 16).

This study does not consider realistic atmospheric forcing. In coupled ocean–atmosphere models (Delworth et al. 1993; Saravanan and McWilliams 1995) the variability in the surface thermal forcing seems to play a much more important role in the excitation of decadal–interdecadal signals than the variability in the $(E - P)$ flux. In the present context the amplitude of the forcing is somewhat arbitrary. We have simply demonstrated that equivalent perturbations in the surface density distribution (induced by either temperature or salinity variations) lead to a similar model response.

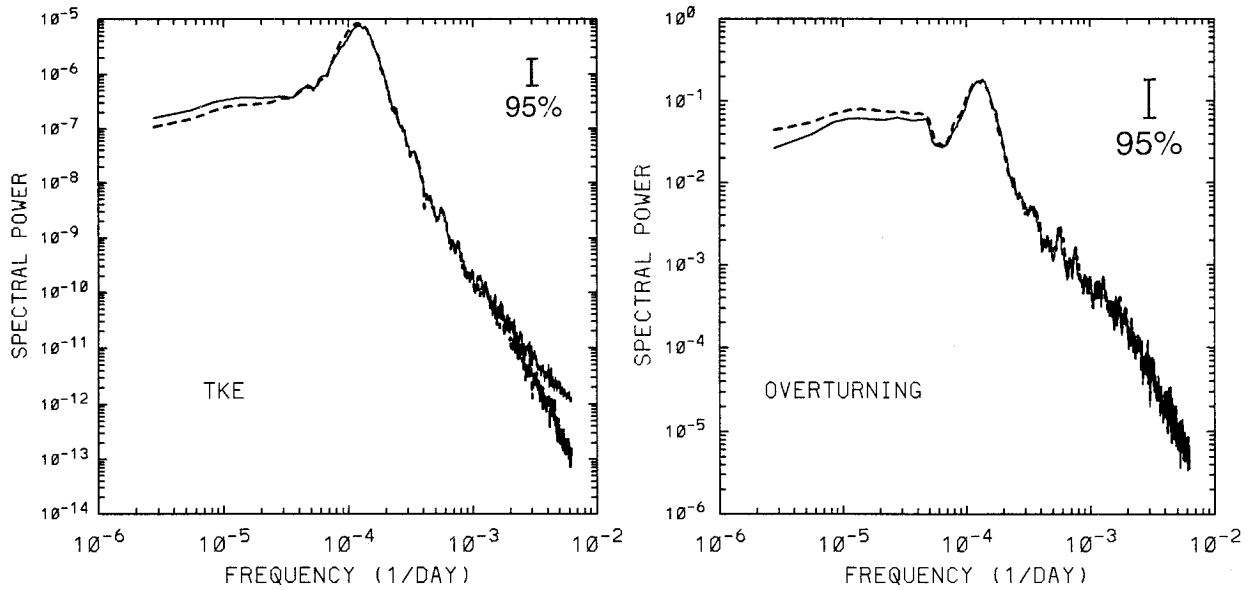

FIG. 18. Frequency spectra of total kinetic energy time series (left) and meridional overturning (right) for the case of freshwater stochastic forcing (solid line) and thermal stochastic forcing (dashed line). In both cases the surface boundary conditions are in flux form for both heat and freshwater and the spatial pattern of stochastic forcing is spatial pattern 1.

e. Effects of nonlinearities in the equation of state

The results described in the previous sections show the crucial role played by high-latitude temperature variations for the occurrence of decadal variability. One may wonder to which extent this result is a consequence of overestimating the effect of temperature at high latitudes by using a linear equation of state. To assess the effect of the nonlinearities in the equation of state on the characteristics of the model variability, we have carried out an experiment in which a quadratic approximation to the equation of state is used. In this experiment we use the FBC thermal boundary condition. We first spin up the model to a steady state starting from the mean state in Fig. 3 as the initial condition. The new steady state (not shown) has a very similar value for the overturning, although the sinking area close to the northern boundary is broader than in the linear case. We then turn on the stochastic forcing in the surface freshwater flux using spatial pattern 1. Results from a 1000-yr simulation are summarized in Fig. 20, where spectra of total kinetic energy and meridional overturning for the quadratic equation of state (dashed line) are compared with the corresponding spectra obtained with the linear equation of state (solid line). A peak at a decadal period is found also in the nonlinear case in both total kinetic energy and overturning spectra. The major differences with respect to the linear case are a reduced amplitude of the peak in the overturning spectrum and a slight shift of the peak to higher frequencies (corresponding to a period of approximately 17 years) in both total kinetic energy and overturning spectra. Thus, variability in the ocean model circulation at decadal timescales, as described by the total kinetic energy, seems to be comparable in amplitude in both the linear and quadratic cases. However, variability in the strength of the meridional overturning is now reduced, probably reflecting the decreased sensitivity of the density field to temperature variations. In the case of the linear equation of state we have shown that the variability at the decadal scale appears to be a mode of the ocean model that can be more or less efficiently excited by different distributions of surface forcing. This seems to be in agreement with the suggestion of Griffies and Tziperman (1995) that decadal variability can be interpreted as a damped oscillatory mode of the ocean model excited by surface atmospheric noise. If this is the case, the nature of the oceanic mode and, in particular, its frequency can be expected to be dependent upon the mean state of the ocean model. Thus, one may speculate that the change in the frequency of the decadal mode when a quadratic equation of state is used can be related to the differences in the corresponding mean state. The main conclusion of this sensitivity experiment is that nonlinearities in the equation state do affect some aspect of the results, in particular, the intensity of the oscillation in some of the model variables as well as its period. However, the existence of the oscillation itself appears to be a robust result.

4. Discussion and conclusions

In this study, we have investigated the existence of possible modes of variability of an (idealized) ocean model and the dependence of the variability upon some aspects of the surface forcing. The variability has been induced in the model by introducing random compo-

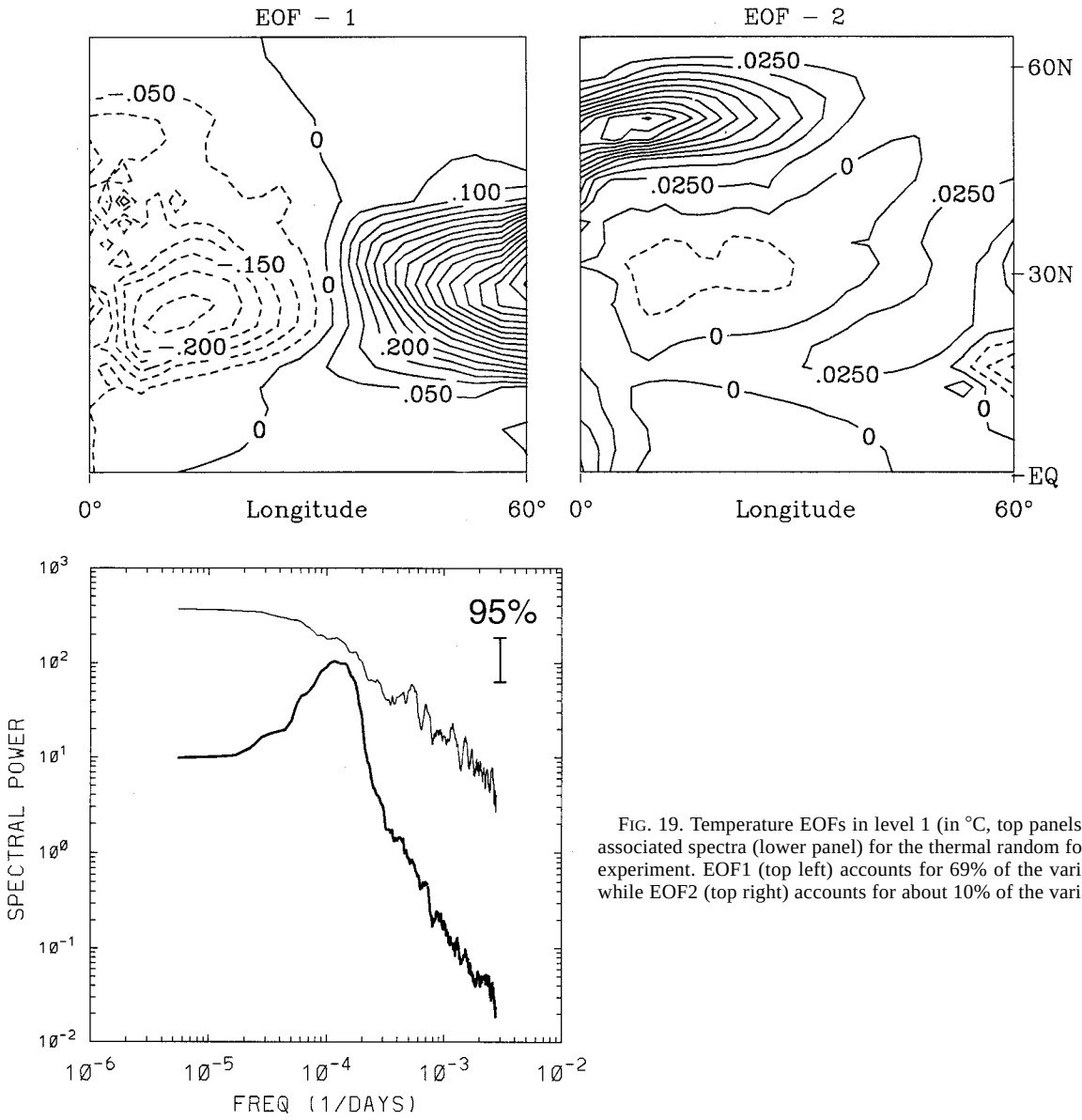

FIG. 19. Temperature EOFs in level 1 (in °C, top panels) and associated spectra (lower panel) for the thermal random forcing experiment. EOF1 (top left) accounts for 69% of the variance, while EOF2 (top right) accounts for about 10% of the variance.

nents in the surface freshwater or heat fluxes. The first aspect of the surface forcing that has been considered concerns the nature of the thermal boundary condition. Several studies (Zhang et al. 1993; Rahmstorf and Willebrand 1995; Mikolajewicz and Meier-Reimer 1994) have shown the extreme sensitivity of the stability of the model meridional overturning to this aspect of the problem, and have demonstrated how thermal boundary conditions that allow the model sea surface temperature to respond to changes in the circulation can considerably enhance the stability of oceanic states. In fact, the possibility for the sea surface temperature to vary allows for a negative (stabilizing) temperature feedback (Rahmstorf and Willebrand 1995) that can counteract the destabilizing positive salinity feedback (Bryan 1986).

Mikolajewicz and Meier-Reimer (1994) discuss some aspects of the influence of surface thermal boundary conditions on the model variability. In this study we have systematically investigated such sensitivity. We have shown that drastic changes in the model variability can be obtained depending upon the degree to which the model sea surface temperature is allowed to vary. Boundary conditions that impose a strong constraint on the model sea surface temperature lead to a type of variability characterized by irregular and dramatic transitions between states of intense overturning and states of almost collapsed overturning. This behavior is char-

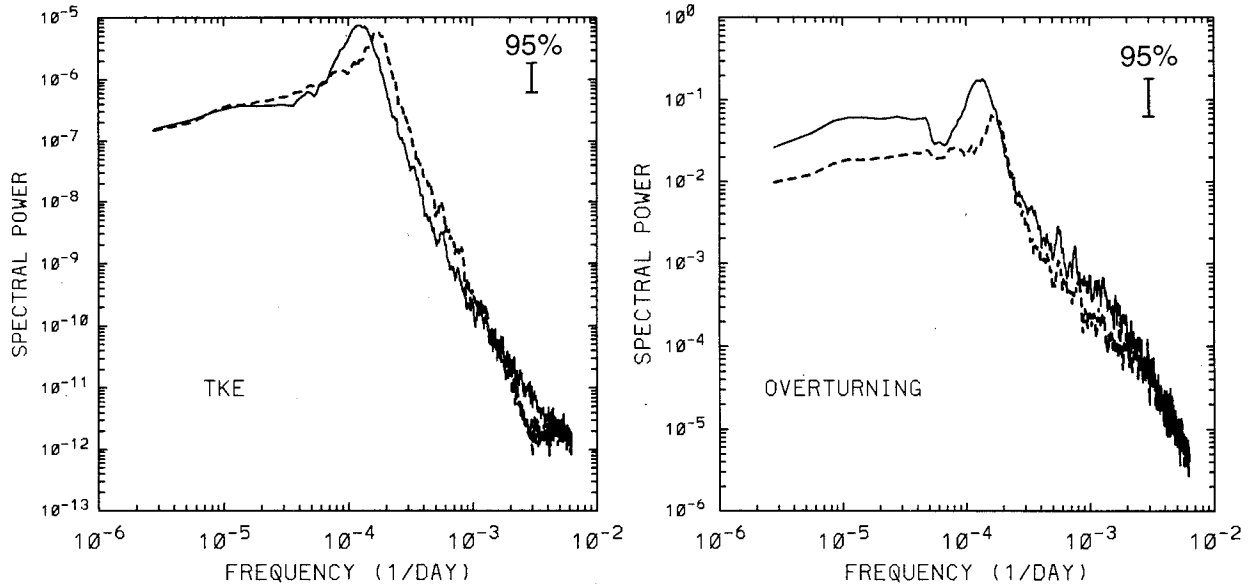

FIG. 20. Frequency spectra of total kinetic energy time series (left) and meridional overturning (right) for the standard case of a linear equation of state (solid line), and for the case of a quadratic equation of state (dashed line). In both cases the surface boundary conditions are in flux form for both heat and freshwater and the spatial pattern of stochastic forcing is spatial pattern 1.

acteristic of flush-type variability, as first described by Marotzke (1989). On the other hand, the possibility for the model sea surface temperature to respond to changes in the circulation allows the occurrence of a quasi-regular and smaller amplitude oscillation at a quasi-decadal period in the intensity of the overturning. The oscillation shows a north–south dipole structure in SST in middle to high latitudes and close to the western boundary, which has a qualitative resemblance with the observed variability in the North Atlantic (Deser and Blackmon 1993; Kushnir 1994). Temperature and velocity anomalies associated with the oscillation are also very similar to the ones found in the GFDL coupled model, as described by Delworth et al. (1993).

The second aspect of the surface forcing that we have considered is the spatial pattern of the stochastic forcing. Low-frequency atmospheric forcing seems to be characterized by spatial coherence, such as the well-known teleconnection patterns (Wallace and Gutzler 1981), and temporal incoherence, the variance spectrum of these patterns being essentially white (Saravanan and McWilliams 1996a). It can be shown (Saravanan and McWilliams 1996b) that the spatial scale of these patterns in the presence of an advective ocean dynamics can give rise to a preferred timescale of variability. For typical values of the atmospheric length scale and oceanic velocity scale, the resulting timescale can be in the decadal range. By choosing spatial patterns with different spatial scales (while keeping the mean oceanic circulation unchanged), we have verified that the (decadal) period of the dominant signal is unaffected by the scale of the forcing, thus excluding the mechanism proposed by Saravanan and McWilliams (1996b). The decadal oscillation appears to be an intrinsic mode of variability of the ocean model, as in the box-model study of Griffies and Tziperman (1995).

Having identified the oscillation as a mode of variability of the ocean model, a question remains about the degree of efficiency of different spatial patterns in exciting this mode. The spatial patterns that we have considered include large-scale (wavenumber 1) forcing of the density gradient in both the zonal and meridional directions as well as smaller-scale forcing (wavenumber 3). While the patterns with larger spatial scales are generally much more efficient in exciting the decadal oscillation, the spatial pattern that directly affects the east–west density (and therefore pressure) gradient appears to give rise to the strongest decadal signal. In fact, since the model ocean circulation is very nearly in geostrophic balance, the east–west pressure gradient directly drives the meridional flow.

Acknowledgments. Conversations with R. Saravanan, C. Deser, J. Hurrell, and R. Greatbatch have been extremely valuable in the development of this study. All the computations have been carried out on SUN sparc stations. We would like to thank T. Vukicevic for making her workstation available for most of the computations. AC has been supported by a CSMP postdoctoral fellowship during the course of most of this work. She has also been partially supported by NOAA Grant DOC-NA56GP02301.

REFERENCES

Anderson, G. E., and J. Willebrand, 1992: Recent advances in modeling the ocean circulation and its effect on climate. *Rep. Prog. Phys.,* **55,** 1–37.

Bretherton, F. P., 1982: Ocean climate modeling. *Progress in Oceanography,* Vol. 11, Pergamon, 93–129.

Bryan, F., 1986: High latitude salinity effects and interhemispheric circulations. *Nature,* **323,** 301–304.

——, 1987: Parameter sensitivity of primitive equation ocean general circulation models. *J. Phys. Oceanogr.,* **17,** 970–985.

Bryan, K., 1969: Climate and the ocean circulation. III. The ocean model. *Mon. Wea. Rev.,* **97,** 806–827.

——, and M. D. Cox, 1972: An approximate equation of state for numerical models of ocean circulation. *J. Phys. Oceanogr.,* **2,** 510–514.

Capotondi, A., and R. Saravanan, 1996: Sensitivity of the thermohaline circulation to surface buoyancy forcing in a two-dimensional ocean model. *J. Phys. Oceanogr.,* **26,** 1039–1058.

Chen, F., and M. Ghil, 1995: Interdecadal variability of the thermohaline circulation and high-latitude surface fluxes. *J. Phys. Oceanogr.,* **25,** 2547–2568.

Cox, M. D., 1984: A primitive equation, 3-dimensional model of the ocean. GFDL Ocean Group Tech. Rep. 1, 56 pp. [Available from Geophysical Fluid Dynamics Laboratory/NOAA, Princeton University, P.O. Box 308, Forrestal Campus, Princeton, NJ 08540.]

Delworth, T., S. Manabe, and R. J. Stouffer, 1993: Interdecadal variations of the thermohaline circulation in a coupled ocean–atmosphere model. *J. Climate,* **6,** 1993–2011.

Deser, C., and M. L. Blackmon, 1993: Surface climate variations over the North Atlantic Ocean during winter: 1900–1989. *J. Climate,* **6,** 1743–1753.

Dickson, R. R., J. Meincke, S. A. Malmherg, and A. J. Lee, 1993: The ''Great Salinity Anomaly'' in the northern North Atlantic 1968–1982. *Progress in Oceanography,* Vol. 20, Pergamon Press, 103–151.

Greatbatch, R. J., and S. Zhang, 1995: An interdecadal oscillation in an idealized ocean basin forced by constant heat flux. *J. Climate,* **8,** 81–91.

Griffies, S. M., and E. Tziperman, 1995: A linear thermohaline oscillator driven by stochastic atmospheric forcing. *J. Climate,* **8,** 2440–2453.

Haney, R. L., 1971: Surface thermal boundary condition for ocean circulation models. *J. Phys. Oceanogr.,* **1,** 241–248.

Hasselman, K., 1976: Stochastic climate models. Part I: Theory. *Tellus,* **28,** 473–485.

Kushnir, Y., 1994: Interdecadal variations in North Atlantic sea surface temperature and associated atmospheric conditions. *J. Climate,* **7,** 141–157.

Levitus, S., J. I. Antonov, and T. P. Boyer, 1994: Interannual variability of temperature at a depth of 125 meters in the North Atlantic Ocean. *Science,* **266,** 96–99.

Lorenz, E. N., 1973: On the existence of extended range predictability. *J. Appl. Meteor.,* **12,** 543–546.

Marotzke, J., 1989: Instabilities and multiple steady states of the thermohaline circulation. *Ocean Circulations Models: Combining Data and Dynamics,* D. T. L. Anderson and J. Willebrand, Eds., Kluwer Academic, 501–511.

Mikolajewicz, U., and K. Maier-Reimer, 1990: Internal secular variability in an ocean general circulation model. *Climate Dyn.,* **4,** 145–156.

——, and ——, 1994: Mixed boundary conditions in ocean general circulation models and their influence on the stability of the model's conveyor belt. *J. Geophys. Res.,* **99,** 22 633–22 644.

Mysak, L. A., D. K. Manak, and R. F. Marsden, 1990: Sea-ice anomalies observed in the Greenland and Labrador seas during 1901–1984 and their relation to an interdecadal Arctic climate cycle. *Climate Dyn.,* **5,** 111–133.

Rahmstorf, S., and J. Willebrand, 1995: The role of temperature feedback in stabilizing the thermohaline circulation. *J. Phys. Oceanogr.,* **25,** 787–805.

Saravanan, R., and J. C. McWilliams, 1995: Multiple equilibria, natural variability, and climate transitions in an idealized ocean–atmosphere model. *J. Climate,* **8,** 2296–2323.

——, and ——, 1996a: Stochasticity and spatial resonance in interdecadal climate fluctuations. *J. Climate,* in press.

——, and ——, 1996b: Advective ocean–atmosphere interaction: An analytical stochastic model with implications for decadal variability. *J. Climate,* in press.

Treguier, A. M., and B. L. Hua, 1987: Oceanic quasi-geostrophic turbulence forced by stochastic wind fluctuations. *J. Phys. Oceanogr.,* **17,** 397–411.

Trenberth, K. E., and C. Guillemot, 1996: Evaluation of the atmospheric moisture and hydrological cycle in the NCEP reanalyses. NCAR Tech. Note TN-430+STR, 300 pp.

Wallace, J. M., and D. S. Gutzler, 1981: Teleconnections in the geopotential height field during the Northern Hemisphere winter. *Mon. Wea. Rev.,* **109,** 784–812.

Weaver, A. J., and E. S. Sarachik, 1991: Evidence for decadal variability in an ocean general circulation model: An advective mechanism. *J. Phys. Oceanogr.,* **21,** 1470–1493.

——, and T. M. C. Hughes, 1994: Rapid interglacial climate fluctuations driven by North Atlantic ocean circulation. *Nature,* **367,** 447–450.

——, J. Marotzke, P. F. Cummins, and E. S. Sarachik, 1993: Stability and variability of the thermohaline circulation. *J. Phys. Oceanogr.,* **23,** 39–60.

——, S. M. Aura, and P. G. Myres, 1994: Interdecadal variability in an idealized model of the North Atlantic. *J. Geophys. Res.,* **99,** 12 423–12 441.

Willebrand, J., 1993: Forcing the ocean with heat and freshwater fluxes. *Energy and Water Cycles in the Climate System,* E. Raschke, Ed., Springer-Verlag, 215–233.

Zhang, S., R. J. Greatbatch, and C. A. Lin, 1993: A reexamination of the polar halocline catastrophe and implications for coupled ocean–atmosphere modelling. *J. Phys. Oceanogr.,* **23,** 1389–1410.